Mammary collective cell migration involves transient loss of epithelial features and individual cell migration within the epithelium

Andrew J. Ewald[1,2,*], Robert J. Huebner[2], Hildur Palsdottir[3], Jessie K. Lee[3], Melissa J. Perez[3], Danielle M. Jorgens[3], Andrew N. Tauscher[3], Kevin J. Cheung[2], Zena Werb[1,‡] and Manfred Auer[3,‡]

[1]Department of Anatomy, University of California-San Francisco, 513 Parnassus Avenue, Box 0452, San Francisco, CA 94143, USA
[2]Departments of Cell Biology and Oncology, Center for Cell Dynamics, Johns Hopkins School of Medicine, 855 N. Wolfe Street, 452 Rangos Building, Baltimore, MD 21205, USA
[3]Life Sciences Division, Lawrence Berkeley National Laboratory, 1 Cyclotron Road, MS Donner, Berkeley, CA 94720, USA
*Author for correspondence (andrew.ewald@jhmi.edu)
‡These authors contributed equally to this work

Accepted 31 January 2012
Journal of Cell Science 125, 2638–2654

doi: 10.1242/jcs.096875

Summary

Normal mammary morphogenesis involves transitions between simple and multilayered epithelial organizations. We used electron microscopy and molecular markers to determine whether intercellular junctions and apico-basal polarity were maintained in the multilayered epithelium. We found that multilayered elongating ducts had polarized apical and basal tissue surfaces both in three-dimensional culture and in vivo. However, individual cells were only polarized on surfaces in contact with the lumen or extracellular matrix. The basolateral marker scribble and the apical marker atypical protein kinase C zeta localized to all interior cell membranes, whereas PAR3 displayed a cytoplasmic localization, suggesting that the apico-basal polarity was incomplete. Despite membrane localization of E-cadherin and β-catenin, we did not observe a defined zonula adherens connecting interior cells. Instead, interior cells were connected through desmosomes and exhibited complex interdigitating membrane protrusions. Single-cell labeling revealed that individual cells were both protrusive and migratory within the epithelial multilayer. Inhibition of Rho kinase (ROCK) further reduced intercellular adhesion on apical and lateral surfaces but did not disrupt basal tissue organization. Following morphogenesis, segregated membrane domains were re-established and junctional complexes re-formed. We observed similar epithelial organization during mammary morphogenesis in organotypic culture and in vivo. We conclude that mammary epithelial morphogenesis involves a reversible, spatially limited, reduction in polarity and intercellular junctions and active individualistic cell migration. Our data suggest that reductions in polarity and adhesion during breast cancer progression might reflect partial recapitulation of a normal developmental program.

Key words: Epithelial morphogenesis, Apico-basal polarity, Mammary gland, Breast cancer

Introduction

Simple epithelial tissues are composed of a single layer of cells connected to each other through intercellular anchoring junctions, including tight junctions, adherens junctions and desmosomes. Epithelial morphogenesis therefore presents a conceptual puzzle, as adhesive junctions and strong apico-basal cell polarity are difficult to reconcile with models of motility derived from the study of isolated fibroblastic cells migrating over flat surfaces (Lauffenburger and Horwitz, 1996; Nelson, 2009). A major barrier to the understanding of mammalian epithelial morphogenesis is that the development occurs deep inside the animal. The mammary gland poses a particular challenge because the developing ductal network is embedded within an adipocyte-rich stroma that scatters light and limits high-resolution imaging. Consequently, mammary ductal morphogenesis has not been directly observed in vivo and the basic events are inferred from analysis of fixed specimens.

The mammary ductal epithelium originates from a multilayered epithelial placode during embryonic development (Hogg et al., 1983). The epithelium internalizes and elongates into the embryonic mesenchyme as a solid, multilayered cord of cells from embryonic days 12–15. Although the mammary cells make extensive cell–cell contacts, they lack many features of mature epithelium, such as tight and adherens junctions (Hogg et al., 1983). During embryonic days 16–20 the epithelium elongates, bifurcates and establishes polarized epithelial architecture with a central lumen and mature junctional complexes (Hogg et al., 1983). This rudimentary ductal network is then essentially inactive until the increase in steroid hormone levels at the onset of puberty. The majority of mammary branching morphogenesis occurs during puberty (Fig. 1A). At the end of embryonic development and at the end of puberty, mammary ducts consist of a highly polarized luminal epithelial cell layer surrounded by myoepithelial cells (Fig. 1B,C). However, ductal elongation during puberty is accomplished by a specialized structure known as the terminal end bud (TEB; Fig. 1D). The TEB contains many luminal epithelial cell layers (Williams and Daniel, 1983), and these cells display incomplete apico-basal polarity as determined by light microscopy (Hinck and Silberstein, 2005; Mailleux et al., 2007; Ewald et al., 2008).

Journal of Cell Science

We developed an ex vivo culture system to enable direct observation of the cell dynamics driving mammary epithelial morphogenesis (Simian et al., 2001; Wiseman et al., 2003; Sternlicht et al., 2005; Fata et al., 2007; Ewald et al., 2008). In the 'organoid' assay we isolate primary mammary epithelial ducts and embed them inside gels of extracellular matrix proteins. Epithelial organoids in three-dimensional (3D) culture initiate, elongate and bifurcate new ducts in a growth-factor-dependent fashion (Fata et al., 2007; Ewald et al., 2008). We used immunofluorescence to verify that the organization and polarity of the epithelium during morphogenesis in 3D culture is highly similar to that in the TEB in vivo (Ewald et al., 2008). We next developed microscopy techniques to visualize the cell dynamics driving mammary morphogenesis in 3D culture (Ewald, 2010). In time-lapse movies we observed a proliferation-dependent transition from a simple to a multilayered epithelial organization and dynamic cell rearrangements within the epithelial layer (Ewald et al., 2008). We did not observe any actin- or membrane-based protrusions extending into the extracellular matrix (ECM). Luminal epithelial buds initiate and elongate as a multilayered epithelium, with active cell rearrangements and without persistent leader cells. As elongation ceases, the epithelium returns to a simple bilayered organization (Ewald et al., 2008). We conclude that the mammary epithelium during morphogenesis in 3D culture is both multilayered and highly dynamic at the cellular level.

Studies in kidney and salivary gland have revealed that epithelial cells exhibit high levels of motility and extensive cell rearrangements during morphogenesis (Larsen et al., 2006; Chi et al., 2009). However, those organs accomplish branching morphogenesis during embryonic development and these cell dynamics are essentially absent by birth (Larsen et al., 2006). Similarly, at the end of puberty all of the TEBs disappear and the mammary ductal network again has a simple bilayered organization and extensive intercellular junctions. However, mammary epithelial fragments isolated from mice of any age will reform TEBs and re-establish a complete ductal epithelial network when transplanted into a cleared mammary fat pad in a host mouse (Daniel et al., 1968). Consistent with these in vivo observations, mammary ducts isolated from embryonic, adolescent and mature mice all branch in 3D organotypic culture and display fundamentally similar cellular dynamics. Mammary epithelial ducts elongate through the action of a multilayered TEB and the epithelium retains the potential to reform TEBs throughout the lifespan. We therefore became specifically interested in determining the extent to which intercellular adhesive junctions and apicobasal polarity are maintained in this transient epithelial multilayer.

The major adhesive junctions in epithelial cells are the tight junctions, adherens junctions and desmosomes. Tight junctions are composed of claudins and occludins and they serve both to control paracellular permeability and to partition the plasma membrane into apical and basolateral domains (Schneeberger and Lynch, 2004). Adherens junctions directly connect cells through classical cadherins and then link cell contacts to the actin cytoskeleton through intracellular catenins (Knudsen and Wheelock, 2005). Desmosomes link cells through desmosomal cadherins and connect these cell contacts to the intermediate filament cytoskeleton (Getsios et al., 2004). In addition to the structural polarity imposed by the localization of the adhesive junctions, epithelial cells also receive molecular polarity information from the apical complex of PAR3, PAR6 and atpical protein kinase C ζ (aPKC-ζ) and basolaterally localized scribble, discs large (DLG) and lethal giant larva (LGL) (Feigin and Muthuswamy, 2009).

Cancer in general, and breast cancer in particular, involves a characteristic loss of apico-basal polarity, changes in cell–cell adhesion, and a transition away from a simple highly polarized epithelia to a multilayered incompletely polarized epithelia (Rosen, 2001; Feigin and Muthuswamy, 2009; Huang and Muthuswamy, 2010). Cell adhesion genes can act as tumor suppressors in mouse models of mammary carcinoma and are frequently mutated in human breast tumors (Berx et al., 1996; Hirohashi, 1998; Conacci-Sorrell et al., 2002; Bogenrieder and Herlyn, 2003; Knudsen and Wheelock, 2005; Derksen et al., 2006; Jeanes et al., 2008; Derksen et al., 2011). Similarly, cell polarity genes can act as tumor suppressors, their loss can cooperate with oncogene function in model systems and their expression and localization is frequently disrupted in human cancers (Bilder et al., 2000; Pagliarini et al., 2003; Pagliarini and Xu, 2003; Feigin and Muthuswamy, 2009; Huang and Muthuswamy, 2010). However, it is unclear whether the changes in cell–cell adhesion and loss of apico-basal polarity observed in cancer are specific features of neoplastic growth or whether normal epithelial morphogenesis also requires reduced polarity and adhesion.

In the present study, we sought to determine whether apico-basal polarity and junctional adhesion were preserved in the multilayered epithelium characteristic of mammary branching morphogenesis. We analyzed the fine structure of mammary epithelium during growth in a 3D organotypic culture model and then the in vivo organization of TEBs during pubertal development. We complemented this ultrastructural analysis with time-lapse microscopy of cell and protrusion dynamics within the epithelial multilayer during morphogenesis in 3D culture.

Results

Mammary epithelial cells can form highly polarized bilayers in Matrigel

We previously established culture conditions sufficient for survival and differentiation of primary mammary epithelium explanted into Matrigel (simple medium: DMEM with F12, insulin-transferrin-selenium and penicillin-streptomycin) in which essentially all epithelial fragments ('organoids') will form bilayered cysts (Fata et al., 2007; Ewald et al., 2008). Addition of nanomolar concentrations of growth factor induces a complex multi-day program of branching morphogenesis (Fata et al., 2007; Ewald et al., 2008). We selected FGF2 for this study as it induces branching morphogenesis with high efficiency (80–95% of organoids) in 3D culture and FGFR2 is required in the TEB during puberty (Lu et al., 2008).

We first sought to define the normal ultrastructural organization of bilayered mammary epithelium in Matrigel. We examined 75 sections from five mammary cysts in simple medium and observed simple epithelial organization by ultrastructure (Fig. 1E). The lumens were electron dense and contained secretory material (black arrows in Fig. 1E–E″). Cells lining the lumen had microvilli (Fig. 1E′) and were connected by tight junctions (Fig. 1E″). We also observed desmosomes connecting luminal–luminal (Fig. 1E′), luminal–myoepithelial (Fig. 1E″) and myoepithelial–myoepithelial cells (not shown). The basal tissue surface was smooth and we detected no protrusions into the ECM.

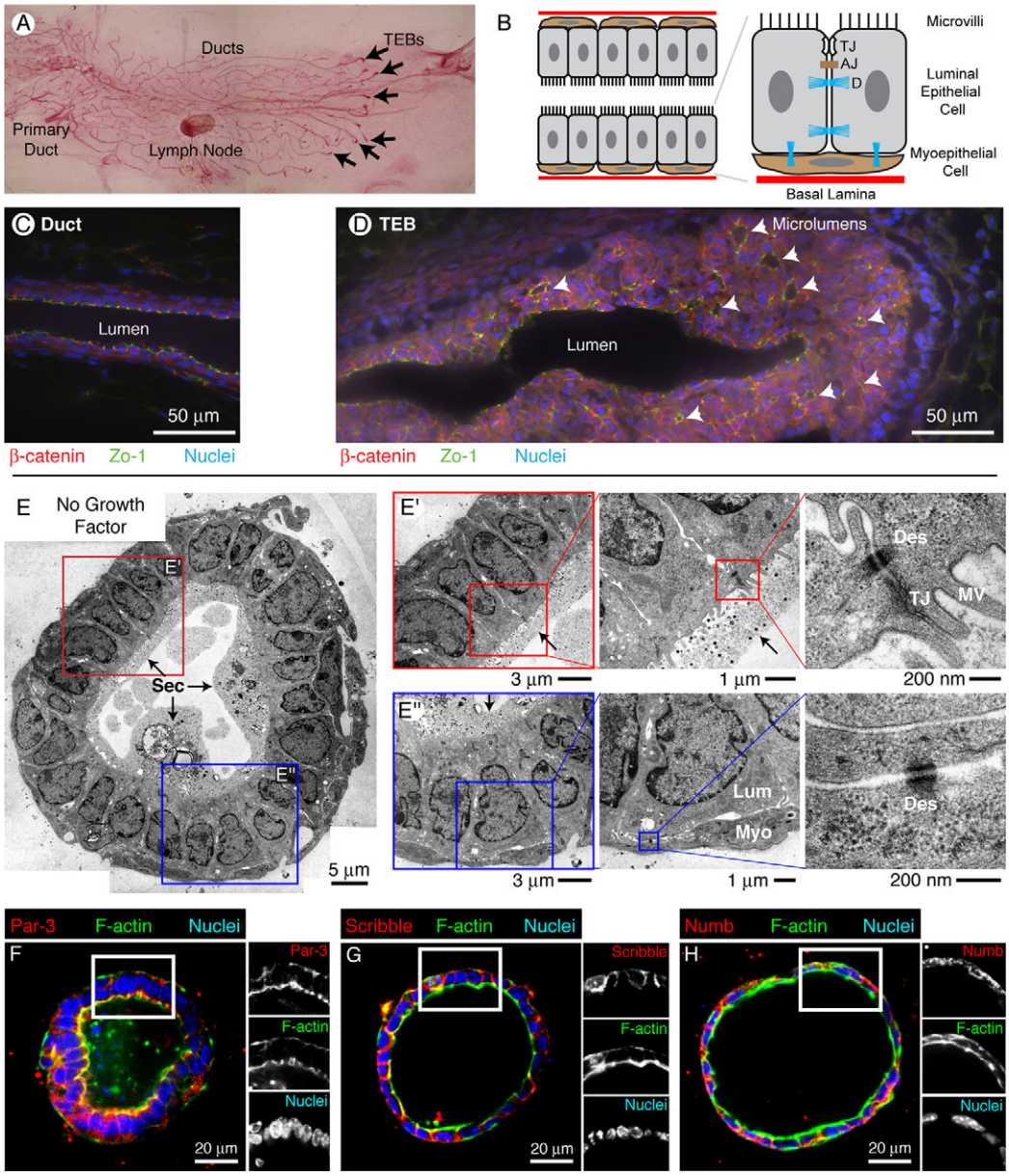

Fig. 1. Normal mammary morphogenesis is accomplished by a stratified epithelium. (**A**) Carmine-Red-stained 10-week-old mouse mammary gland. Mammary ducts are elongated during puberty by specialized structures at the end of the duct, terminal end buds (TEBs). (**B**) Resting mammary ducts have a bilayered organization, with luminal epithelial cells, connected by extensive intercellular junctions, and basally located myoepithelial cells. (**C**) Normal ducts in vivo have a simple epithelial organization when not actively growing. Zona occludens 1 (ZO-1) is localized to the apico-lateral surface of the luminal epithelial cells and β-catenin to the basolateral surfaces. (**D**) Mammary ducts are elongated during puberty by TEBs, stratified epithelial structures with many luminal cell layers. β-catenin localizes to all basolateral surfaces and is only excluded from lumen-facing surfaces. ZO-1 localizes to the lumen lining surfaces of both the main lumen and isolated micro-lumens. (**E**–**E″**) Primary mammary ducts can be isolated and grown in 3D Matrigel gels. Without the addition of growth factor all ducts form simple cysts. These cysts are bilayered, with a single luminal (Lum) cell layer and a single myoepithelial (Myo) layer. The lumen has electron dense secretory material (arrows), microvilli (MV), and tight junctions (TJ). Both luminal and myoepithelial cells are connected by desmosomes (Des). (**F**–**H**) Polarized cysts in 3D culture localize PAR3 to apical surfaces (F) and both scribble (G) and numb (H) to basolateral surfaces. All TEM images are from high-pressure frozen, freeze-substituted samples that were pre-fixed with 4% glutaraldehyde.

Morphological polarity can be assessed with transmission electron microscopy (TEM), but molecular polarity is most readily assayed with immunofluorescence. Simple epithelial polarity is associated with apical localization of the PAR3–PAR6–aPKC-ζ complex and basolateral localization of scribble. Consistent with the high degree of morphological polarity observed by TEM, the molecular polarity complexes were also segregated into distinct apical and basolateral domains. PAR3 was apically localized on the lumen-facing surface of the luminal epithelial cells (Fig. 1F), whereas scribble was basolaterally localized in the luminal epithelial cells (Fig. 1G). The protein numb is involved in cell polarity, adhesion (Wang et al., 2009) and asymmetric cell division in multiple systems (Gönczy, 2008). In polarized bilayers its localization is confined to the basolateral

domain (Fig. 1H). We therefore conclude that our epithelial isolation and culture conditions in Matrigel are compatible with simple epithelial organization, complete apical junctional complexes and fluid-filled lumens, consistent with the in vivo organization of mammary ducts in the mouse (Pitelka et al., 1973) and human mammary glands (Ozzello, 1971; Stirling and Chandler, 1976; Stirling and Chandler, 1977).

Mammary morphogenesis in 3D culture is accomplished via a transiently stratified epithelium

Mammary epithelium in 3D culture forms a multilayered epithelium that initiates, elongates and bifurcates new mammary buds (Ewald et al., 2008). Apico-basal polarity is well defined in simple epithelia (Ozzello, 1971; Pitelka et al., 1973; Nelson, 2009), but the extent of polarity within the interior of a transiently multilayered epithelium was unclear. We have previously shown that aPKC-ζ localizes to all interior contact surfaces within the multilayer suggesting that interior cells lack segregated apical and basolateral membrane domains (Fig. 2A) (Ewald et al., 2008). Following morphogenesis, the localization of aPKC-ζ in the re-established simple epithelium is restricted to the apical surface (Fig. 2A′) (Ewald et al., 2008). We have also shown that E-cadherin and β-catenin localize to all interior contact surfaces within the multilayer, both in vivo and in vitro (Fig. 2B–C′) (Ewald et al., 2008). Because E-cadherin and β-catenin are major components of the adherens junction these data

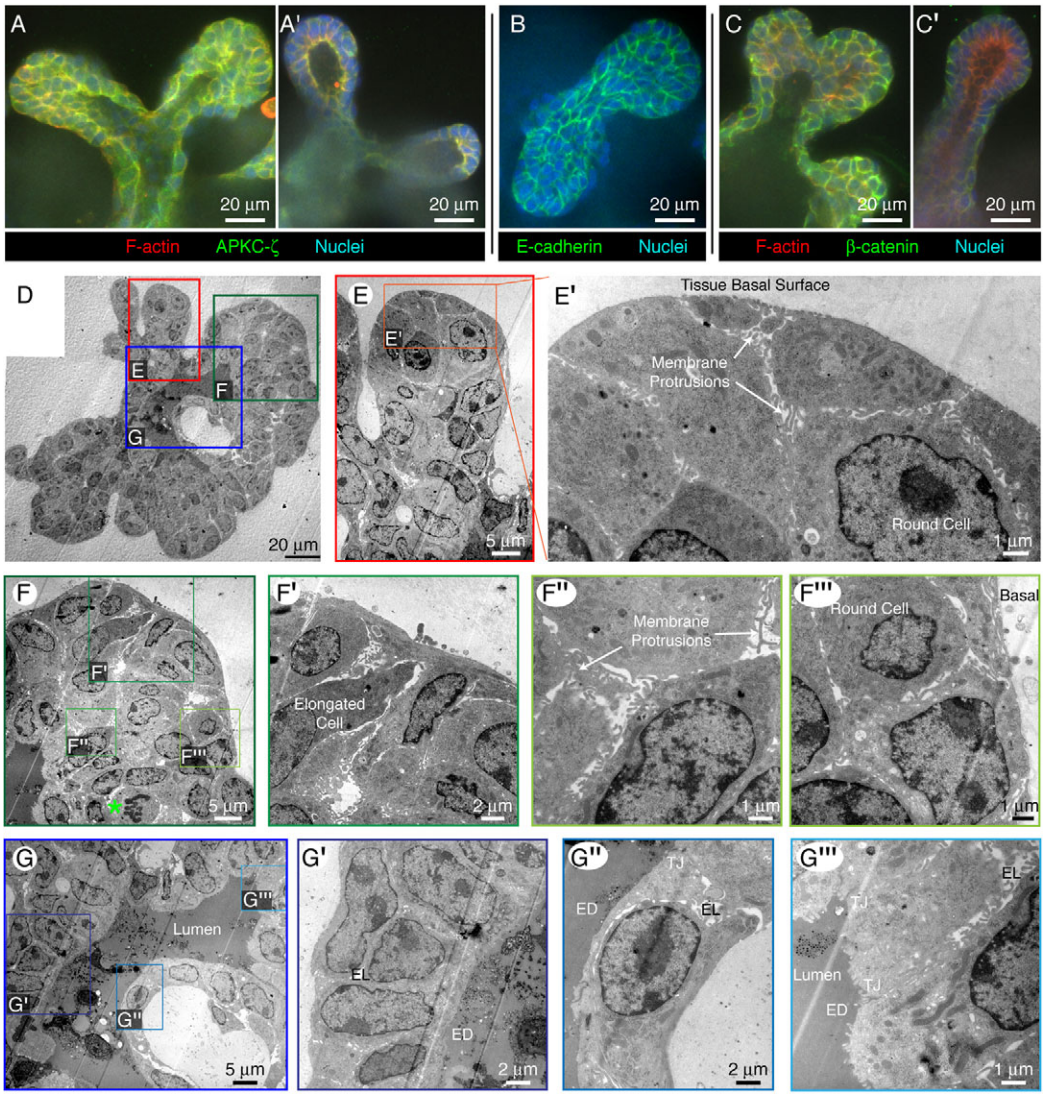

Fig. 2. During morphogenesis in 3D culture the mammary epithelium is transiently stratified. (**A**–**C′**) Within the multilayered epithelium of elongating buds in 3D culture, most interior cell surfaces are not in contact with the lumen or the ECM. These interior surfaces stained positive for aPKC-ζ (A), E-cadherin (B) and β-catenin (C). Following morphogenesis, the mammary epithelium regained a simple organization. In regions of simple organization, aPKC-ζ localized to apical domains (A′) and β-catenin localized to basolateral domains (C′). (**D**–**E′**) TEM was used to define the ultrastructural polarity of the tissue. The basal tissue surface was smooth and lacks ECM-directed protrusions. (**F**–**G‴**) Both elongated cells (F') and round unpolarized cells (F‴) are present in the interior of the multilayer. Away from the basal tissue surface, the epithelial cells exhibit dense, inter-digitating membrane extensions (F″). We also observed division of round cells distant from either the ECM or lumen facing surfaces (F, green asterisk). (**G**–**G‴**) Within the same branching structure, there are regions with simple epithelial organization with an electron-dense lumen and tight junctions. All TEM images are from high-pressure frozen, freeze-substituted samples that were pre-fixed with 4% glutaraldehyde. ED, electron dense; EL, electron lucid; TJ, tight junction.

motivated us to assay for junctional complexes directly. Here, we used TEM and further molecular marker analysis to test our hypothesis that mammary morphogenesis involves a transient reduction in apico-basal polarity and junctional adhesion in interior cells.

Mammary epithelium during morphogenesis lacks protrusions into the ECM

A newly discovered feature of mammary collective epithelial migration is the absence of forward-oriented actin protrusions in advance of elongating ducts (Ewald et al., 2008). However, it was possible that fine protrusions extended into the ECM that could not be detected by light microscopy. To test for fine protrusions, we fixed organoids during active branching and identified regions of active ductal elongation on the basis of the organization of the epithelium. We examined 95 sections from 12 samples. We typically observed ducts elongating simultaneously in multiple directions (Fig. 2A–D). We then examined the basal surface of elongating ducts in 3D culture at high resolution by TEM. We saw no evidence of forward-oriented protrusions into the ECM (0 of 95 sections, Fig. 2D–F). We instead observed a smooth and organized basal tissue surface. Individual cells showed polarized basal surfaces at the tissue–ECM interface, but little morphologically evident polarity on interior surfaces (Fig. 2F–F‴).

Mammary epithelial morphogenesis in 3D culture involves a reduction in intercellular junctions

Because cells in the interior of the multilayer did not have conventional epithelial cell morphologies, we next sought to determine the extent to which intercellular junctions are maintained during normal branching morphogenesis. We observed well-defined apical tissue surfaces, with electron-dense lumens, microvilli and extensive secretory material (Fig. 2D,G–G‴). Tight junctions only connected cells lining electron-dense luminal spaces (TJ in Fig. 2G″,G‴). We observed an electron-dense luminal space and an electron-lucid intercellular space between cells in the multilayered region (Fig. 2G″,G‴). By contrast, cells within the interior of the multilayered epithelium lacked most features of simple epithelial organization or apico-basal polarity. We did not observe a zonula adherens at points of interior cell–cell contact. However, E-cadherin and β-catenin were still membrane localized in interior cells and so we cannot rule out the possibility of small E-cadherin-based adhesive complexes that would be difficult to detect by TEM. Cell–cell contact in the interior appeared loose and was characterized by extensive frequently interdigitating membrane extensions (Fig. 2F″). Interior cells displayed a variety of cell shapes and sizes and frequently included round cells with minimal cell–cell contacts (Fig. 2F‴).

Interior cells lack membrane-associated PAR3 and are unpolarized

Because the interior cells lacked morphological polarity, we next used antibodies to visualize the localization of molecular markers for apico-basal polarity during each stage of morphogenesis in 3D culture. Interior cells within the multilayered epithelium displayed a diffuse cytoplasmic localization of PAR3 (Fig. 3A). By contrast, scribble was membrane-associated on all interior cell surfaces in the multilayer and was absent only from lumen-facing surfaces (Fig. 3B). Similar to the localization of scribble, numb was localized to all lateral surfaces at the complex cyst stage. In the multilayered epithelium of elongating ducts, PAR3 localized to all lumen-facing membranes, but was diffusely localized to the cytoplasm in interior cells (Fig. 3D). Scribble and numb instead localized to all interior cell surfaces and were excluded from lumen-facing surfaces (Fig. 3E,F). After morphogenesis, the

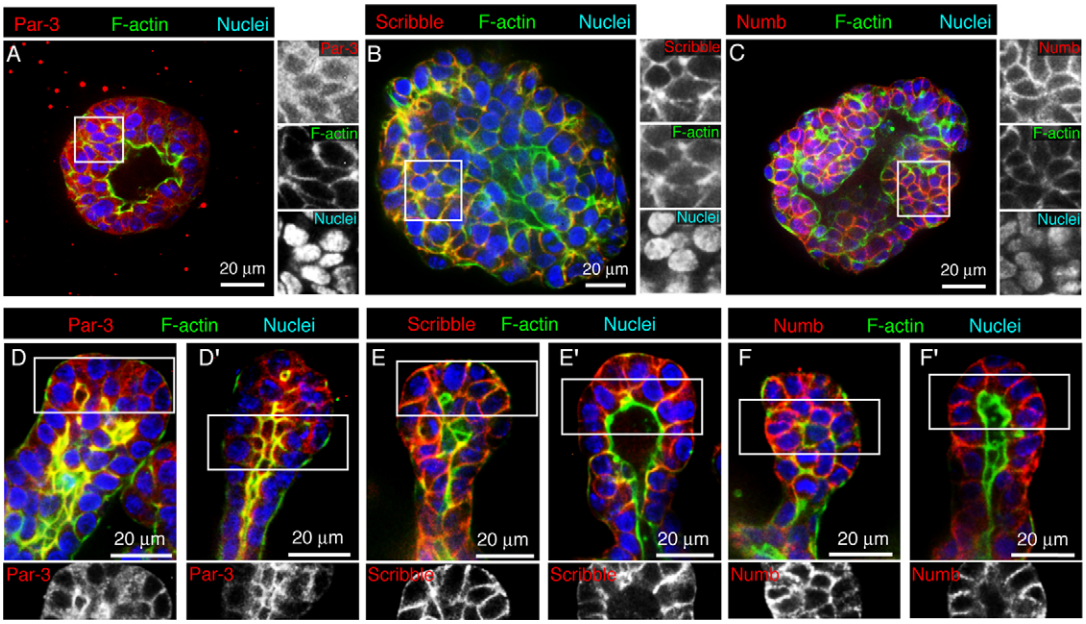

Fig. 3. Morphogenesis in 3D culture is associated with a loss of molecular polarity. (**A**–**C**) Interior cells are first evident in 'complex cyst' structures. Within these structures interior cells display cytoplasmic localization of PAR3 (A), whereas scribble and numb localize to all interior cell surfaces (B,C). (**D**–**F′**) In the multilayered region of elongating mammary end buds PAR3 is cytoplasmically localized (D), whereas scribble and numb localize to all interior surfaces. After morphogenesis is complete the epithelium regains a simple epithelial organization and PAR3 is associated with the apical membrane (D′), whereas scribble and numb are localized to basolateral cell surfaces (E′,F′).

reformed simple epithelium had PAR3 that was localized to the apical surface of luminal cells and scribble and numb to basolateral surfaces (Fig. 3D′,E′,F′).

Isolated microlumens exist between interior cells in the multilayered epithelium in 3D culture

We have previously observed small isolated zona occludens protein 1 (ZO-1; also known as TJP1)-lined spaces within the multilayered epithelium of elongating mammary buds both in 3D culture and in vivo (Ewald et al., 2008). We sought to distinguish whether these represent small lumens or accumulations of apical molecular markers without corresponding ultrastructural features. We first used confocal microscopy to collect optical sections and generate 3D reconstructions of the multilayered mammary epithelium during 3D culture. We discovered that the ZO-1-lined microlumens were isolated from the main lumen of the organoid (Fig. 4A–A″). Following morphogenesis, individual ducts had single simple lumens (Fig. 4B,B′). Using TEM we observed both empty (electron lucid) intercellular regions (Fig. 4C′) and isolated lumens filled with electron-dense material (Fig. 4C″–D‴). The electron-lucid intercellular regions had extensive membrane protrusions but no evidence of tight junctions or secretory material (Fig. 4C′, white arrow). Desmosomes were the only junctions that we observed connecting cells surrounding the electron-lucid intercellular spaces. By contrast, isolated microlumens had microvilli, as well as tight junctions at points of apical intercellular contact and accumulated electron-dense material (Fig. 4C″–D‴). Isolated lumens extended several microns into the multilayer (Fig. 4E).

Epithelial organization is highly variable during morphogenesis in 3D culture

Our expectation was that cells at the basal tissue surface would remain columnar throughout branching. Strikingly, this was not the case and we observed considerable heterogeneity in the shape of basally located cells (Fig. 5A), with ‘islands’ of high local order (Fig. 5A′) and disorder (Fig. 5A″) located in the same branching structure. Even in actively branching structures with highly variable cell shapes, there were frequently locations with a single luminal epithelial cell layer and highly polarized ultrastructural organization. Following branching the transiently stratified epithelium returned to a simple epithelial organization, with mature apico-basal polarity at the morphological level.

Regions with few intercellular junctions display extensive 3D membrane protrusions

During active morphogenesis in 3D culture, we observed few intercellular junctions connecting interior cells, but extensive membrane protrusions. Some of these protrusions had the morphological appearance of interdigitating microvilli (Fig. 5B,B′). However, membrane protrusions were observed at some distance from the apical surface and were frequently

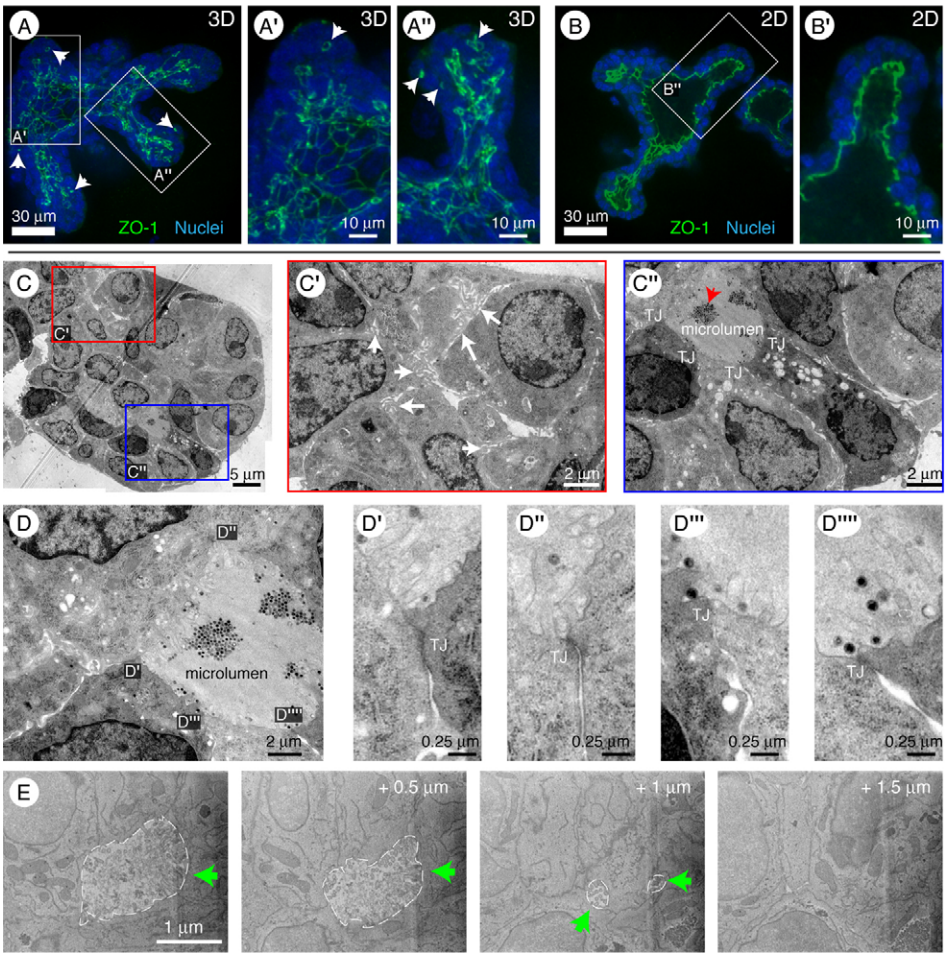

Fig. 4. The multilayered region contains microlumens with tight junctions. (**A**–**A″**) Light microscopy of the multilayered region. ZO-1 (green) localizes both to the lining of the main lumen and to isolated microlumens located between luminal epithelial cells (arrowheads in 3D volume reconstruction). (**B**,**B′**) Following morphogenesis a simple epithelial organization is restored and a single clear lumen is observed. (**C**–**D‴**) Using TEM there are two different intercellular spaces: electron-lucid spaces with extensive irregular membrane protrusions but without tight junctions (C′, white arrows) and electron-dense intercellular spaces with tight junctions (TJ), microvilli and secretory material (red arrow in C″) (C″–D‴). (**E**) Serial block face scanning electron microscopy enabled 3D reconstruction of the microlumens and confirmed that they are several microns thick. All TEM images are from high-pressure frozen, freeze-substituted samples that were pre-fixed with 4% glutaraldehyde. The image series used to generate E has been uploaded to ‘The Cell: An Image Library’.

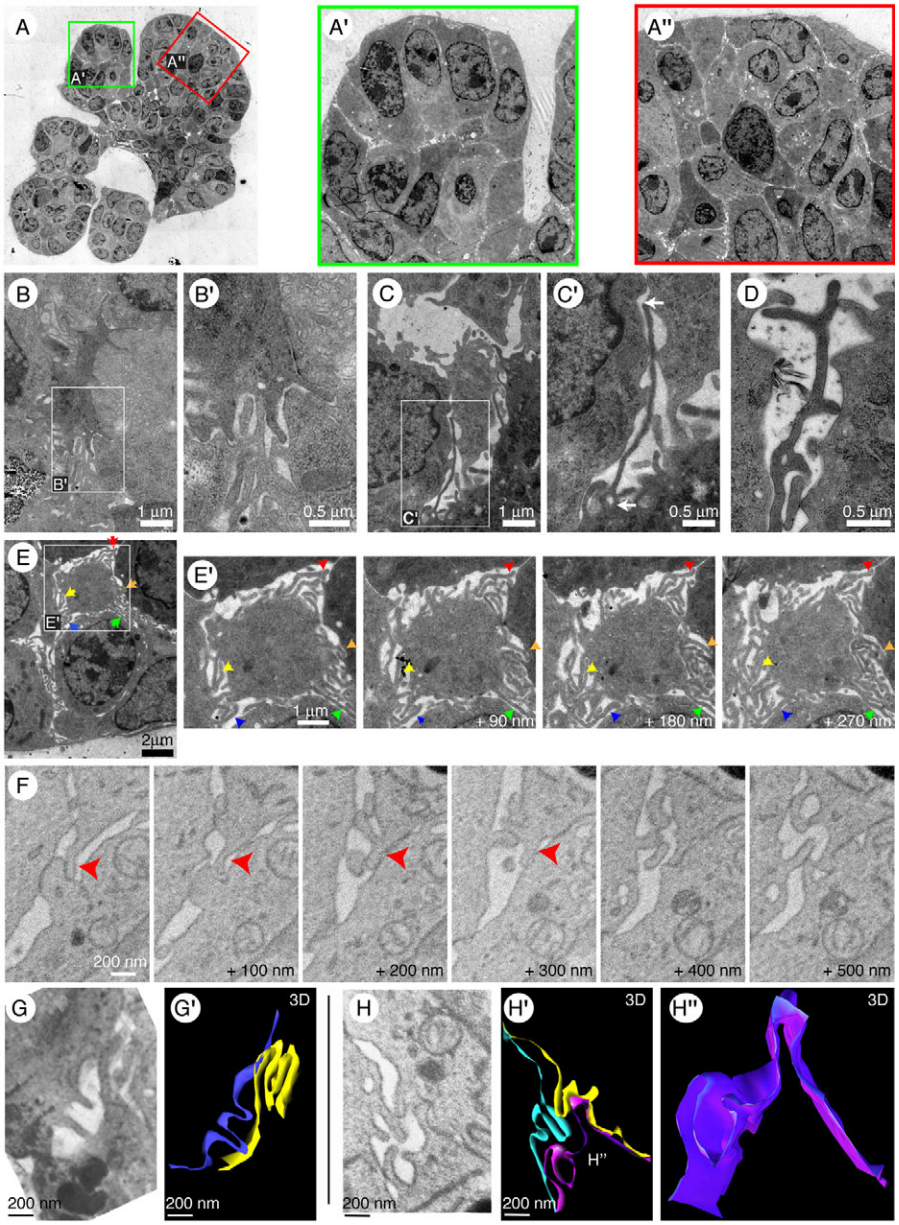

Fig. 5. Cell shape and lateral membrane organization are highly heterogeneous in the multilayered region. (**A**–**A″**) Nearby regions in the same branching structure can have high (A′) or low (A″) epithelial organization. (**B**–**D**) Lateral membrane protrusions within the multilayer were frequently interdigitated (B–B′), could be several microns in length (C–C′) and were frequently branched (D). (**E**–**F**) Analysis of serial sections by TEM (E,E′) and serial block face scanning electron microscopy (F) revealed that the lateral membrane protrusions extend through multiple sections (colored arrowheads) and can morph between thin and broad and between linear and branched. (**G**–**H″**) Three-dimensional reconstructions of cell contact regions along interior lateral surfaces using serial block face SEM revealed densely interdigitating 3D membrane extensions. All TEM images are from high-pressure frozen, freeze-substituted samples that were pre-fixed with 4% glutaraldehyde. The image series used to generate F has been uploaded to 'The Cell: An Image Library'.

intermixed with desmosomes. Membrane protrusions were several microns in length (Fig. 5C,C′) and branched multiple times (Fig. 5D). The uniform thickness along the protrusions, as well as the tendency for the protrusions to appear continuous over long distances, led us to analyze whether they were thin microvillar-like individual membrane protrusions or whether they were complex 3D membrane extensions. Accordingly, we collected a series of consecutive 90-nm sections and imaged each by TEM (Fig. 5E,E′; supplementary material Fig. S1A). Protrusions extended through 5–10 sections and changed continuously from branched to unbranched (Fig. 5E′, arrowheads).

To confirm the 3D structure of these newly discovered membrane protrusions we next collected continuous image series using serial block face scanning electron microscopy (SFB-SEM) and focused ion beam scanning electron microscopy (FIB-SEM). In both cases, a thin layer of material was removed from the surface of the embedded sample and the block face was then imaged. The procedure was repeated to produce a 3D image series. Serial block face and focused ion beam imaging both prevent warping artifacts associated with transfer of a thin section to a solid support. We observed transitions from thin to thick protrusions and from linear to branched protrusions (Fig. 5F; supplementary material Fig. S1B, Fig. S2). We conclude that these membrane elements are interdigitating 3D membrane extensions (Fig. 5G–H″). By contrast, we did not observe complex 3D extensions in regions of simple epithelial organization.

Interior cells exhibit apparently migratory polarity during morphogenesis in 3D culture

As ductal elongation ceases, the multilayered duct reorganizes to a simple epithelium (Ewald et al., 2008). In electron micrographs, this corresponded with a transition from largely non-junctional cell adhesion with loose cell–cell contact to a simple epithelial

organization with extensive intercellular junctions. One possible mechanism for a transition from a multilayered to simple organization is radial intercalation, in which cells move between layers to give a thinner tissue (Keller, 2002; Stubbs et al., 2006). We observed elongated cells within the multilayered epithelium whose morphology was consistent with individualistic cell migration (Fig. 6A–D). Despite the absence of actin-based protrusions extending into the ECM, we observed long extensions at the front of these elongated cells (Fig. 6A,B). One cell that appeared to have recently arrived at the basal surface displayed an intermediate polarity between elongated and apico-basal (Fig. 6D–D″).

Desmosomes are frequently observed in the interior of the multilayered epithelium

We have demonstrated that a subset of cells in the interior of the multilayered epithelium lack molecular apico-basal polarity and appear to have a migratory polarity and forward-oriented

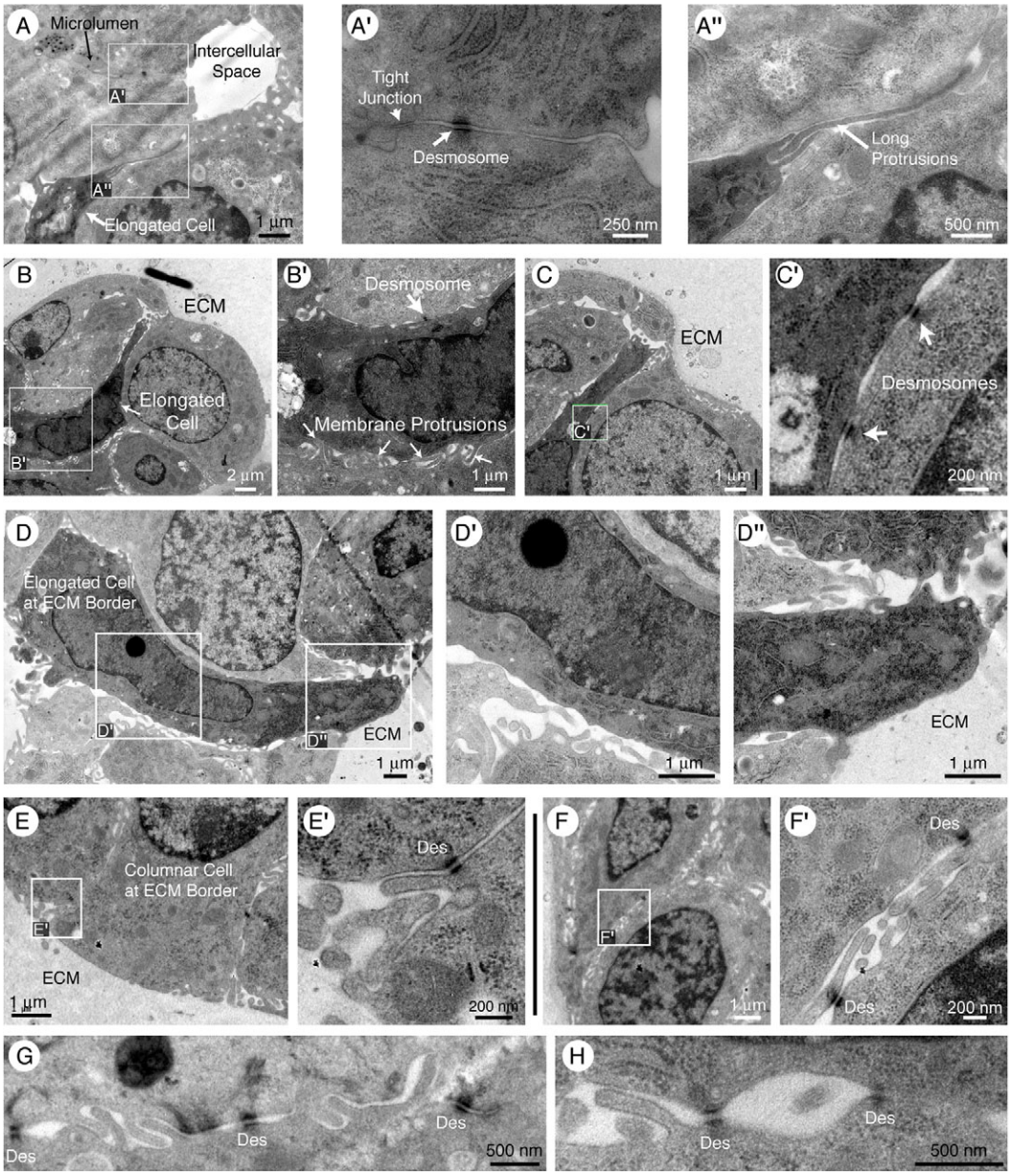

Fig. 6. Elongated cells are observed within the epithelial multilayer. (**A**–**A″**) Electron-dense elongated cells are seen within the multilayered region. These cells frequently have long protrusions extending in a single direction between adjacent cells (A″). (**B**–**C′**) Elongated cells were observed deep within the multilayer (A) and also within microns of the ECM (B). The only intercellular junctions observed on these cells were small desmosomes (C–C′). (**D**–**D″**) At the ECM border some cells had an appearance that was intermediate between columnar epithelial and elongated morphologies. They did not extend protrusions into the ECM. (**E**–**F′**) Cells in extensive contact with the ECM had smooth basal surfaces and lateral desmosomes, but frequently displayed little morphologic polarity on their lateral surfaces. (**G**–**H**) Interior cells have lateral surfaces with intermixed membrane protrusions and small desmosomes. All TEM images are from high-pressure frozen, freeze-substituted samples that were pre-fixed with 4% glutaraldehyde.

protrusions. However, we did not observe spontaneous dissemination of luminal epithelial cells in 3D culture in the hundreds of movies we collected in our previous study (Ewald et al., 2008). We therefore sought to identify persistent intercellular junctions that might limit the dissemination of luminal epithelial cells. The only intercellular junctions that we regularly observed connecting interior cells during morphogenesis were desmosomes (Fig. 6B′–C′,E–H). We observed desmosomes connecting apparently migratory cells to their neighbors in close proximity to the ECM (Fig. 6B–C′). We also observed desmosomes connecting columnar cells at the ECM border (Fig. 6E–F′) and interior cells within the multilayer (Fig. 6G,H). Desmosomes in the interior were small and did not accumulate extensive intracellular plaques to the degree observed in highly polarized epithelial cells (compare Fig. 6G,H with Fig. 1E′,E″).

Interior cells are protrusive and migratory within the multilayered epithelium

Our electron micrographs revealed extensive protrusions and apparent migratory polarity in cells within the epithelial multilayer. However, it is difficult to infer cell movements accurately from a series of fixed specimens. We therefore labeled small numbers of cells using adenovirally delivered cytoplasmic GFP and imaged their behavior using time-lapse confocal microscopy. We tracked 21 cells from 10 movies collected over three independent experiments. All 21 cells were protrusive and motile. Cells had a mean speed of 5.5±1.8 μm per hour (±s.d.).

We observed individual cells migrating over multiple cell diameters within the multilayered epithelium (Fig. 7A; supplementary material Movie 1). Round cells in the interior extended and retracted long cytoplasmic protrusions (Fig. 7B; supplementary material Movie 2). We also directly observed radial intercalation of front–rear-polarized migratory cells into the tissue basal surface (Fig. 7C; supplementary material Movie 3). The forward extensions in these cells immediately flattened out as the cells made contact with the extracellular matrix. Cells just inside from the tissue basal surface extended and retracted protrusions over most of their cellular surface area (Fig. 7D; supplementary material Movie 4). Cells bridging tissue apical and tissue basal surfaces also extended and retracted protrusions along their lateral surfaces (Fig. 7E; supplementary material Movie 5). We did not observe protrusions into the ECM or the lumen. We conclude that mammary epithelial cells display extensive protrusions during morphogenesis in 3D culture on all interior cell surfaces and that individual cells appear to migrate actively in the interior of the multilayer.

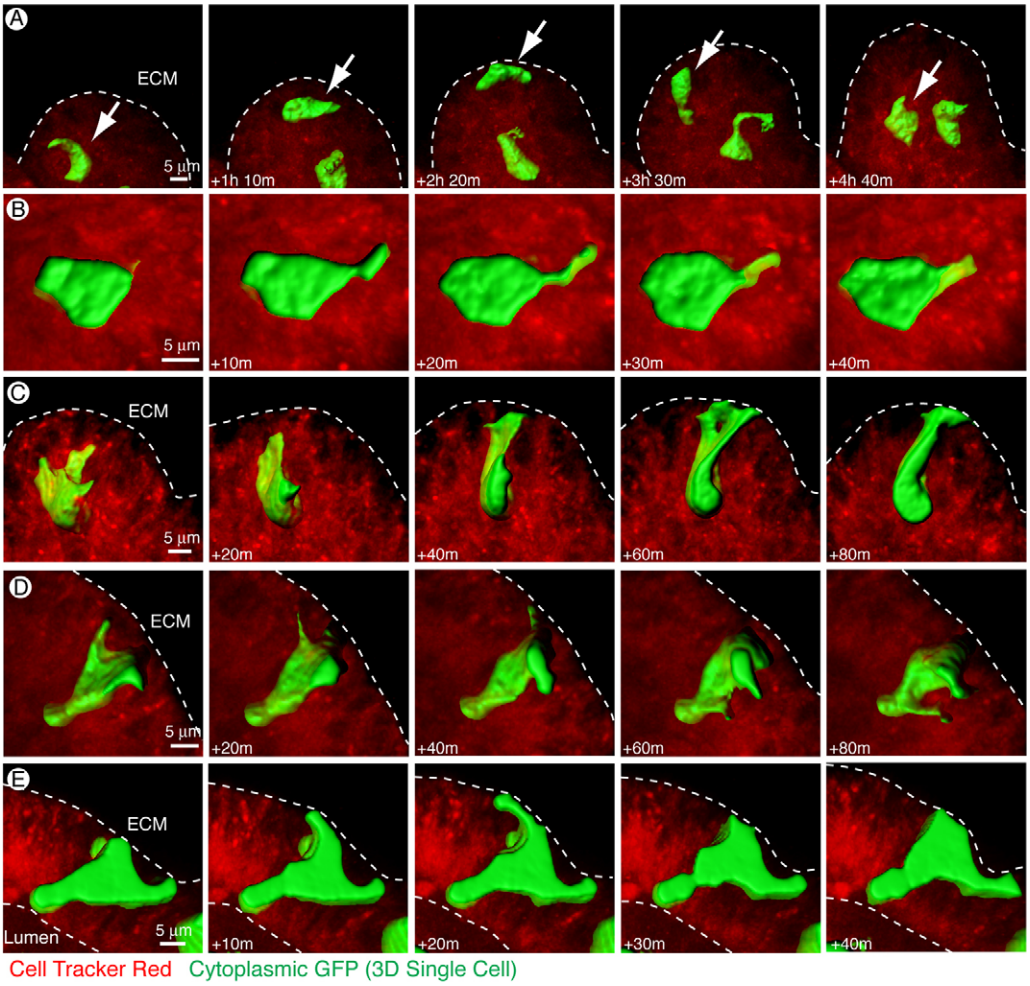

Fig. 7. Interior cells are frequently migratory and protrusive within the multilayer. All cells were labeled with Cell Tracker Red and a subset of cells were labeled with an adenovirally delivered cytoplasmic GFP. Images depict 3D reconstructions of the cytoplasm in individual GFP-positive cells. (**A**) Interior cells were frequently highly migratory and could move in directions opposite to the direction of ductal elongation. (**B**) Interior cells extended and retracted cytoplasmic protrusions within the multilayer, but not into the lumen or ECM. (**C**) Individual cells migrated from the interior to basal positions in contact with the ECM, a process termed radial intercalation. (**D**,**E**) Cells in contact with the basal tissue surface (D) or both apical and basal tissue surfaces (D,E) extended cytoplasmic protrusions from all lateral surfaces. The movies used to generate A–E are presented in supplementary material Movies 1–5, respectively.

Inhibition of MLCK or Rac blocks duct initiation but results in different architectural states

Pharmacological inhibition of either Rac or myosin light chain kinase (MLCK) results in a dose-dependent block of ductal initiation (Ewald et al., 2008). In both cases, when we added the inhibitor at the start of culture the lumens fill as normal, but new ducts do not initiate. However, inhibition of Rac results in a persistently multilayered epithelium, whereas MLCK-inhibited structures eventually clear their lumens to form a simple epithelial organization (Ewald et al., 2008). Accordingly, we examined organoids treated with 100 µM Rac inhibitor and collected electron micrographs to determine whether these structures were well polarized (two samples, 220 sections imaged; supplementary material Fig. S3). We observed extensive cell–cell contact through interdigitating membrane protrusions. By contrast, organoids treated with 1 µM MLCK inhibitor (ML7) cleared their lumens and their final ultrastructural organization was indistinguishable from simple cysts (one sample, 16 sections imaged; supplementary material Fig. S3).

ROCK inhibition prevents reversion to the single layered state and results reduced interior cell-cell contact

Pharmacologic inhibition of Rho kinase (ROCK) with Y-27632 results in a hyper-branched phenotype with reduced levels of E-cadherin at intercellular surfaces (Ewald et al., 2008). On the basis of the lower intensity and punctate appearance of E-cadherin staining following inhibition of ROCK, we hypothesized that

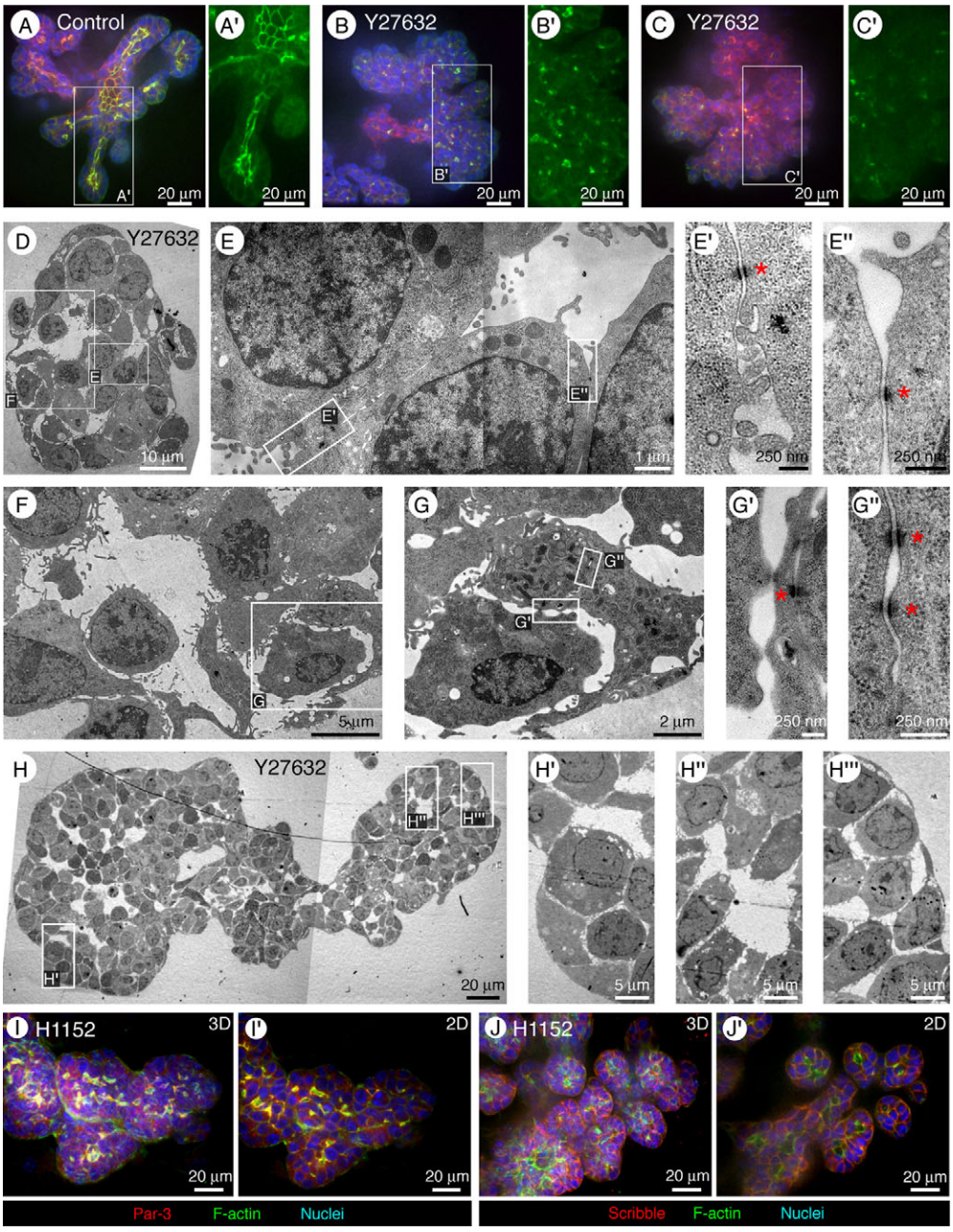

Fig. 8. Treatment with Y-27632 results in disorganization and reduced cell–cell contact on lateral and apical surfaces. (**A–C′**) Normal organoids have a stereotyped branching pattern, with a large ZO-1-lined lumen (A,A′). Treatment with the ROCK inhibitor Y-27632 results in rapid loss of the lumen, luminal epithelial disorganization and localization of ZO-1 exclusively to small foci (B,B′). Large regions of Y-27632-treated epithelium were free of ZO-1 immunoreactivity (red, phalloidin; green, ZO-1; blue, nuclei). (**D–H‴**) Ultrastructural examination revealed a loss of electron-dense luminal spaces and a large decrease in cell–cell contact along lateral cell surfaces. The basal tissue surface was still smooth and well organized (H–H‴). The only junctions we observed connecting cells in Y-27632-treated samples were small desmosomes (red asterisks, E′,E″,G′,G″). All TEM images are from high-pressure frozen, freeze-substituted samples that were pre-fixed with 4% glutaraldehyde. (**I,I′**) Organoids treated with the ROCK inhibitor H1152 had microlumen-localized PAR3 (I, 3D reconstruction; I′, 2D optical section). (**J,J′**) Organoids treated with H1152 had lateral-surface-localized scribble but no scribble on the microlumen surface (J, 3D reconstruction; J′, 2D optical section).

Y-27632 treatment disrupts cell–cell contacts between luminal epithelial cells. Indeed, we observed dramatic changes in the localization of ZO-1 in ROCK-inhibitor-treated organoids (compare Fig. 8B–C′ with Fig. 8A,A′). Following ROCK inhibition, ZO-1 was frequently associated with small puncta (Fig. 8B′), but large regions that lacked ZO-1 immunoreactivity were also observed (Fig. 8C′). Consistent with these observations, we observed a striking reduction in intercellular contact in TEM images of ROCK-inhibited organoids (Fig. 8D–H‴; two samples, 34 sections imaged). Lumens were no longer observed and cell–cell contacts were barely maintained on lateral surfaces (Fig. 8D,F). We essentially observed a complete loss of luminal organization with no tight or adherens junctions. Instead of electron-dense lumens, there were electron-lucid intercellular spaces. Interior cells barely contacted each other and appeared completely unpolarized. Despite this dramatic loss of polarity and the reduction in cell–cell contact, we still observed occasional small desmosomes (Fig. 8E′,E″,G″) and a well-organized basal tissue surface (Fig. 8H–H‴). This dramatic reduction in polarity and adhesion is reversible (Ewald et al., 2008) and was not sufficient for dissemination of interior cells into the ECM. Treatment with H1152, an alternate ROCK inhibitor, also induced loss of the main lumen and extensive microlumens (Fig. 8I,J; supplementary material Fig. S4). However, some apico-basal polarity was maintained in H1152-treated organoids as PAR3 localized to the membrane of the microlumens (Fig. 8I,I′), whereas scribble localized to basolateral surfaces and was excluded from the microlumens (Fig. 8J,J′). We conclude that ROCK (or another Y27632-sensitive kinase) is required for maintenance of luminal continuity and lateral cell–cell adhesion within the luminal epithelial cell layer.

Terminal end buds in vivo have similar organization to mammary organoids.

Given the highly unusual ultrastructural organization of mammary epithelium during branching morphogenesis in 3D culture, we next asked whether the morphology of the interior cells of branching organoids matched the organization of interior (‘body’) cells of the normal in vivo structure for mammary ductal elongation, the TEB. We collected electron micrographs of

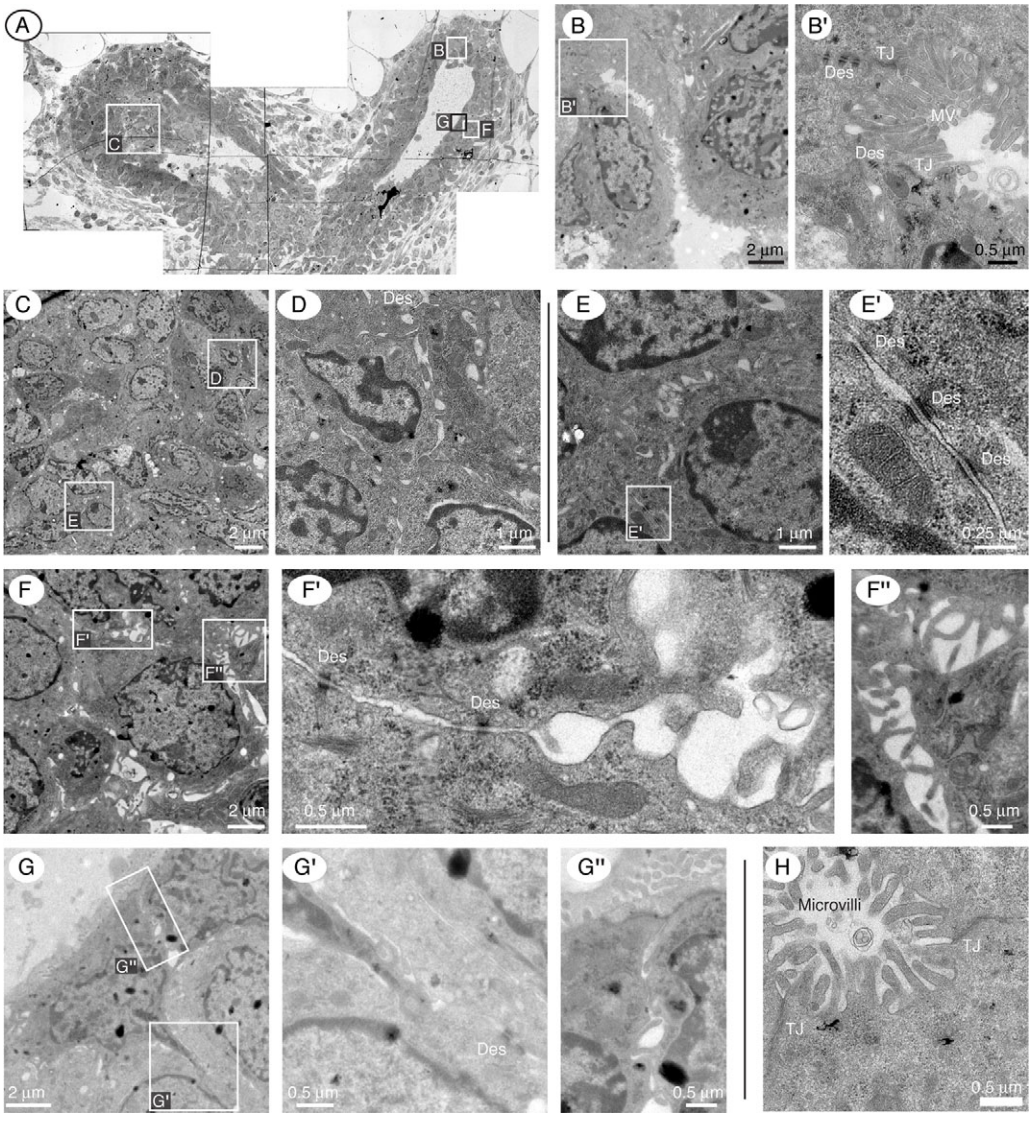

Fig. 9. TEBs in vivo display reduced apico-basal polarity and extensive intercellular membrane protrusions. (**A**) Mammary epithelial ducts are elongated by TEBs, shown here in a light micrograph, with boxes indicating regions that were subsequently imaged by TEM. (**B**,**B′**) TEBs contain a fluid-filled lumen with microvilli and tight junctions. (**C**–**F″**) Cells within the multilayered region appeared morphologically unpolarized and displayed extensive intercellular protrusions. These protrusions were observed to interdigitate (D) and branch (F″). (**G**–**G″**) Cells at the apical or basal most tissue surface were polarized at the tissue boundary but could be unpolarized and irregularly shaped a few microns away. (**H**) Microlumens within the body cell region had both microvilli and tight junctions. All TEM images are from high pressure frozen, freeze-substituted samples that were pre-fixed with 4% glutaraldehyde. Des, desmosomes; TJ, tight junctions.

sections through TEBs, including regions at the cell–ECM, lumen-facing and interior surfaces (Fig. 9; four samples, 60 sections imaged). Consistent with our in vitro results, we observed tight junctions connecting cells at surfaces facing lumens (Fig. 9B,B′). We also did not observe protrusions from the basal TEB surface into the ECM. As in the 3D cultures, there was considerable heterogeneity in cell and nuclear morphologies in the TEB (Fig. 9C). Body cells of TEBs had a similar cellular organization to interior cells in 3D culture, with extensive interdigitating lateral membrane protrusions (Fig. 9D–F″). The TEB was polarized at its apical and basal most tissue surfaces, with many morphologically unpolarized cells in the interior (Fig. 9C–F). Furthermore, the morphological polarity of cells lining the lumen was generally restricted to the lumen-facing surface, with interior surfaces adopting a round or mesenchymal morphology (Fig. 9G–G″). We also observed microlumens within the multilayered region of the TEB, both by light (Fig. 1D) and electron microscopy (Fig. 9H).

Discussion

The mammary gland undergoes multiple rounds of epithelial morphogenesis during puberty, pregnancy, lactation and involution (Hennighausen and Robinson, 2005; Sternlicht, 2006). The mammary epithelium at rest has a simple organization, with a single luminal epithelial cell layer (Ozzello, 1971; Pitelka et al., 1973). During early embryonic development and during puberty the elongating tips of mammary ducts are multilayered (Hogg et al., 1983; Williams and Daniel, 1983; Ewald et al., 2008). In this study, we used molecular markers and TEM to determine the polarity and adhesional status of this multilayered intermediate. Interior cell surfaces within the multilayered localized both apical (aPKC-ζ) and basolateral (scribble) molecular markers. Despite E-cadherin and β-catenin localization, we did not observe zonula adherens connecting interior cells. Instead points of cell–cell contact in the interior were connected by desmosomes and characterized by extensive interdigitating 3D membrane extensions. Interior cells were observed to extend protrusions and to migrate, but these behaviors were transient and spatially limited to the interior of the multilayer (Fig. 10).

3D primary organotypic culture recapitulates the normal junctional adhesion of the mammary epithelium

Without growth factor stimulation primary mammary organoids in 3D culture robustly form cysts with a highly polarized bilayered architecture and microvilli lining the lumen. The epithelium developed a complete apical junctional complex and displayed extensive desmosomal connections along lateral surfaces. This organization is consistent with the normal ultrastructure of the mammary epithelium in vivo (Pitelka et al., 1973), and is in contrast to the ultrastructural organization of MCF-10A acini cultured under similar 3D culture conditions. MCF-10A cysts do not form detectable tight junctions and instead appear to form their lumens through extensive desmosomal contacts (Underwood et al., 2006). Our primary 3D cultures therefore provide a starting point for mechanistic evaluation of the relative importance of different junctional complexes and adhesion proteins.

Mammary epithelium adopts a low polarity state with few junctions during morphogenesis

During morphogenesis, the mammary epithelium was polarized at its apical (lumen-facing) and basal (ECM-contacting) tissue surfaces. However, even cells at the lumen or ECM border typically were polarized only on their apical- or basal-most cell surfaces. Cells in the interior were loosely connected and displayed dense interdigitating membrane protrusions. Some of these protrusions appeared morphologically similar to microvilli, despite their interior location. Other protrusions were intermingled with desmosomes in electron-lucid intercellular spaces, were several microns long, or were branched, all features uncharacteristic of classical microvilli. In volume reconstructions, these protrusions appeared as an interconnected 3D network of membrane extensions, rather than individual thin projections. Because we observed similar membrane protrusions on interior cells in TEBs from normal mammary glands, we conclude that these structures are transiently produced both in vivo and in vitro during normal mammary morphogenesis. These 3D membrane extensions increase the entangled surface area of adjacent cells and we speculate that they might thereby assist in maintaining intercellular adhesion among motile cells.

Tight junctions are only observed lining lumens

Tight junctions classically serve two functions: gate and fence. They function as a gate to enable selective control over paracellular permeability. They also function as a fence within the membrane, partitioning the apical from basolateral membrane regions (Nelson, 2009). Previous work has established that TJs can exist in stratified epithelia (Langbein et al., 2002), but we found no evidence for TJs in the interior of the multilayer during morphogenesis except at the apical end of cells facing lumens. Without TJs in the interior of the multilayer, it is consistent that the membranes appear to have an unresolved mix of apical and basolateral identity.

Mammary epithelial cells display extensive protrusive activity and individualistic cell migration within the multilayer

Elongating mammary buds maintain a smooth and highly organized basal-tissue–ECM surface both in vivo and in 3D culture. However, we observed extensive protrusions in the interior of the epithelium. We did not observe protrusions into the ECM at either the light or electron microscopy levels. These observations imply that there is a reduction in the epithelial

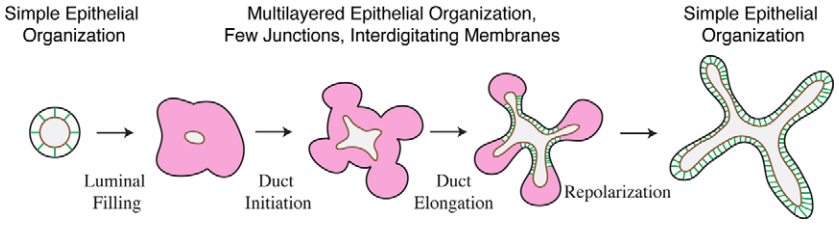

Fig. 10. Normal mammary epithelial morphogenesis is accomplished via a transiently stratified epithelium. The transient multilayered epithelium associated with mammary morphogenesis is polarized as a tissue but displays reduced apico-basal polarity and few intercellular junctions at points of cell–cell contact in the interior.

character of mammary epithelial cells during morphogenesis, as protrusive migration is characteristic of mesenchymal cells. Strikingly, this reduction was spatially restricted to the multilayered region within elongated ducts and was reversible, with normal ducts eventually reverting to bilayered organization.

Epithelial organization during morphogenesis is similar in 3D culture and in vivo

The low intercellular adhesion, reduced polarity environment that we observed during morphogenesis in organotypic culture is highly similar to the organization of the in vivo mammary terminal end bud (TEB). The essential features of reduced intercellular adhesion, reduced apico-basal polarity, fewer intercellular junctions and stratified epithelial organization are all quite similar between organoids and TEBs. We observed tight junctions at the apical end of cells facing microlumens, and desmosomes connecting cells in the electron lucid intercellular spaces in both TEBs and ducts in 3D culture. Significantly, the low polarity environment is also similar to that observed in the mammary placode during embryonic development (Hogg et al., 1983; Nanba et al., 2001). Whereas our data directly address only mouse mammary morphogenesis, immunohistochemistry of sections from pubertal human mammary epithelium, and human TEBs, indicates that a similar multilayered intermediate underlies human mammary morphogenesis (Rudland, 1991).

There are extensive previous TEM studies of simple bilayered mammary ducts (Ozzello, 1971; Pitelka et al., 1973), but we are aware of only one previous study that has used TEM to image TEBs during puberty (Williams and Daniel, 1983). In that study the authors observed membrane protrusions into intercellular spaces between interior cells within the TEB, consistent with our results. More recent TEM studies in the mammary gland have proposed that small light-staining cells are stem or progenitor cells (Smith and Medina, 1988; Chepko and Smith, 1997; Chepko and Smith, 1999; Smith and Chepko, 2001). We also observed variation in electron density, with smaller rounder cells typically staining more lightly, and larger elongated cells typically staining darker.

Collective epithelial migration has features of the epithelial to mesenchymal transition

A primary model for the cellular mechanism of normal and neoplastic epithelial morphogenesis is the epithelial to mesenchymal transition (EMT). Morphological hallmarks of this model include a reduction in epithelial organization and acquisition of motility. EMT has been proposed to explain the dissemination of previously adherent epithelial cells into the surrounding ECM and is thought to be a major cellular mechanism of metastasis in human breast cancer (Kalluri and Weinberg, 2009; Polyak and Weinberg, 2009). We did not observe migration of interior cells into the ECM either in 3D culture or in vivo. However, the reduced epithelial polarity and intercellular adhesion and increased motility that we observed during morphogenesis are consistent with models of a partial transient EMT (O'Brien et al., 2002). However, we observed a striking confinement of these migratory cells to the interior of the multilayer.

Furthermore, most models propose that EMT occurs at the epithelial–stromal or tumor–stromal border (Lee et al., 2011). We see the opposite; the highest level of E-cadherin staining and the ultrastructurally highest degree of epithelial organization is at the luminal and basal surfaces of the tissue. It is the interior multilayered epithelial compartment, which is out of contact with ECM and stromal cells, that exhibited the largest reduction in epithelial character. Furthermore, the cellular phenotype associated with inhibition of ROCK suggests that the luminal and lateral intercellular adhesions can be essentially eliminated without dissemination or loss of basal tissue organization.

Desmosomes are the most common junction connecting cells in the interior of the multilayered epithelium

Research in epithelial biology has focused on the adherens junction in part because E-cadherin is required very early in embryonic development (Larue et al., 1994) and disruption of the adherens junction can lead to disruption of the other adhesive junctions (Gumbiner et al., 1988). However, disruptions in desmosomal adhesion can also have severe phenotypes and can alter the function of classical cadherin junctions (Green and Gaudry, 2000; Vasioukhin et al., 2001; Den et al., 2006; Lechler and Fuchs, 2007). Desmosomes were the main intercellular junction that we observed in the interior of the multilayered epithelium both in 3D culture and in vivo. Desmosomes were also the only junction we observed connecting elongated, apparently migratory cells to their neighbors. A previous TEM study of cells in the interior of the elongating embryonic mammary bud found very few junctional complexes connecting interior cells, but did observe desmosomes (Hogg et al., 1983). The requirement for desmosomal adhesion has not been tested genetically in the mammary gland, but 3D culture studies suggest that desmosomal cadherins are essential to establish and maintain the correct apico-basal positions of luminal and myoepithelial cells (Runswick et al., 2001). Furthermore, desmosomal components are frequently mutated or silenced in breast cancer (Klus et al., 2001; Oshiro et al., 2005), and both p53 and p63 can regulate desmosomal adhesion (Ihrie and Attardi, 2005; Cui et al., 2011; Dusek and Attardi, 2011).

Epithelial polarity and adhesion are altered during cancer progression

Both normal and neoplastic mammary epithelia lose polarity, reduce adhesion and shift from a simple to a multilayered organization. Importantly, normal mammary epithelia reduce the amount of polarity and adhesion in a highly restricted space for a limited period of time, whereas mammary carcinomas persist in a state with lower polarity and adhesion. The reversibility of even very large changes in adhesion and polarity in normal epithelia suggest that tumors might also be able to 'correct' their organization and revert to a normal tubular architecture given the right set of molecular signals. In fact, previous work spanning over several decades has shown that human tumors can be 'normalized' by contact with embryonic mesenchyme and by contact with cell-type specific extracellular matrix proteins (Streuli et al., 1991; Petersen et al., 1992; Weaver et al., 1997; Nelson and Bissell, 2006; Hendrix et al., 2007; Ingber, 2008; Weigelt and Bissell, 2008).

A previous ultrastructural study has examined ductal hyperplasias, ductal carcinoma in situ and infiltrating ductal carcinomas from human patients to determine the basis of the invasive switch in human breast cancer (Goldenberg et al., 1969). Importantly, the authors reported that: "The most notable finding in our ultrastructural study of various types of breast lesions was an increased degree of cell membrane anomaly paralleling the increased degree of aggressiveness among these lesions…

atypical ductal hyperplasia was characterized by abundant microvilli… [i]ntraductal carcinomas were recognizable by extremely complex cell interdigitations. Infiltrating ductal carcinomas were detectable by an overabundance of cellular microvilli" (Goldenberg et al., 1969). The morphological similarity between the complex interdigitations in the intraductal carcinomas in that study and in the normal mammary cells undergoing morphogenesis in our study is striking and suggests that at least some human breast cancers might recapitulate aspects of a normal developmental migration program. We have demonstrated in the present study that the ultrastructural organization of mammary epithelium during postnatal morphogenesis is highly similar to that during embryonic morphogenesis (Hogg et al., 1983). This observation provides an ultrastructural framework for the hypothesis that there is an embryonic program of partial EMT that can be reactivated during postnatal development and during cancer progression (Yang and Weinberg, 2008).

Conclusions

Normal mammary morphogenesis involves a shift from a simple to a multilayered organization, dynamic cell movements and reduced apico-basal polarity. In this study, we have defined a new ultrastructural basis for the 'morphogenetically active epithelial state' adopted during developmental remodeling of the mammary gland. It is now important to understand the nature of the molecular signals that enable this transition to be highly regulated in space and time during normal development. In particular, cell–cell adhesion is strikingly altered during morphogenesis, with few observed intercellular junctions and extensive entangled membranes. At present we do not know the relative contributions of classical and desmosomal cadherin systems to cell–cell adhesion during mammary morphogenesis. Another major challenge is to define the cellular and molecular mechanisms by which polarized epithelial cells reversibly create a multilayered epithelium with lower levels of polarity.

Materials and Methods

Organotypic culture

We generated epithelial fragments ('organoids') as previously described (Ewald et al., 2008; Ewald, 2010), using 5- to 8-week-old Charles River FVB mice as the source material. For ease of dissection, TEBs were isolated from a 5-week-old fluorescent reporter transgenic mouse (Sca-1::EGFP) (Hanson et al., 2003). Animals were housed and handled in accordance with approved IACUC protocols at UCSF or JHU. Briefly, to generate organoids we surgically isolated the mammary glands, minced them ~50 times with a scalpel and dispersed the glands for 30 minutes in 50 ml collagenase solution at 37℃, shaking at 100 rpm. The resulting mixture was then centrifuged at 520 ***g*** for 10 minutes at 25℃. We aspirated away the supernatant and resuspended the pellet thoroughly in 4 ml DNase solution. We shook the tube by hand for 2 to 5 minutes at room temperature and then added 6 ml DMEM F12. We then centrifuged at 520 ***g*** for 10 minutes at 25℃ and aspirated the supernatant. To separate the epithelial organoids from the single cells we used differential centrifugation, a total of 4 times. For each round we resuspended the pellet thoroughly in 10 ml DMEM F12 and then pulsed the tube to 520 ***g*** (typically 33 seconds). The resulting pellet was then resuspended in the desired volume of growth factor reduced Matrigel (BD Biosciences) and plated in 24-well not tissue-culture treated plates (Falcon). Organoids were grown for 5–6 days and then fixed during the time active branching morphogenesis was ongoing.

Solutions and reagents for organotypic culture

DMEM (Dulbecco's modified Eagle's medium complete) F12 (Gibco). Collagenase solution consisted of: DMEM F12, fetal bovine serum (FBS, heat inactivated) (5% final), gentamicin (50 µg/ml), insulin (5 µg/ml final, Sigma), trypsin (2 mg/ml, Gibco), collagenase A (2 mg/ml, Type IV from *Clostridium histolyticum*, Sigma). DNase I (Sigma) was resuspended at 4 U/ml in DMEM F12. Bovine serum albumin (BSA; Invitrogen) was resuspended at 2.5 mg/ml in D-PBS. Simple medium: DMEM F12, 1× Pen-Strep, 1× ITS (insulin, transferrin, sodium selenite; Sigma). Branching medium: simple medium plus 2.5 nM FGF2 (Sigma). ROCK inhibitor (Y27632; Chemicon) and Rac1 inhibitor (NSC23766; Calbiochem) were used as indicated. All inhibitor experiments were done in FGF2 medium.

Fixation strategy for ultrastructural analysis

We initially utilized conventional chemical processing and transmission electron microscopy (TEM) and observed minimally adherent cells, with highly convoluted membranes and extensive intercellular spaces. However, we encountered inadequate and irregular cytoplasmic and membrane preservation (not shown). These limitations in tissue preservation are often associated with room temperature dehydration and can be overcome by high-pressure freezing and subsequent freeze substitution (McDonald and Auer, 2006). However, fresh tissue microdissection and the exposure of unfixed tissues to relatively high levels of cryoprotectants (e.g. 20% glycerol), just prior to high-pressure freezing, can lead to physical damage or osmotic stress (Triffo et al., 2008). To avoid aggregation artifacts caused by the dehydration step in conventional protocols, yet guard against osmotic stress in fresh dissected tissue sample upon exposure to cryoprotectants, we adopted a conservative approach to sample preparation. We first prefixed in glutaraldehyde, then microdissected prefixed samples, then processed the samples for high-pressure freezing and freeze substitution (Sosinsky et al., 2008). Using this combination we were able to achieve high-quality ultrastructural preservation across large sample regions. On separate samples, we also employed serial block face SEM to allow 3D reconstruction of selected regions of interest to identify the intercellular membrane protrusions. Our focus was on the membrane organization and junctional complexes, both of which were well preserved in our samples. Given the highly heterogeneous epithelial environment in our samples, it was crucial to be able to process and image large areas of the samples to enable both low-magnification surveys of fields of cells and higher-resolution imaging of individual points of cell–cell contact. Three biologically independent sets of samples were examined for the main FGF2-treated branching organoids. Parallel samples were examined with conventional chemical processing TEM. The conclusions were consistent across all samples, but membrane preservation was better with high-pressure freezing and freeze-substitution prepared samples. All images presented are from samples subjected to high-pressure freezing.

High-pressure freezing

Samples were pre-fixed overnight in 4% glutaraldehyde in organoid medium. They were then subjected to high-pressure freezing in a BAL-TEC HPM-010 high-pressure freezer (2100 bars for 5–7 milliseconds) (BAL-TEC, Carlsbad, CA) using 10% glycerol (v/v in cell culture medium) as the cryoprotectant in 200-µm deep aluminum planchettes.

Freeze substitution

Using the Leica automated freeze-substitution system AFS (Leica Microsystems, Vienna, Austria), cryofixed specimens were freeze-substituted in anhydrous acetone containing 1% osmium tetroxide and 0.1% uranyl acetate and after several rinses in pure acetone infiltrated with Epon-Araldite following established protocols (McDonald and Müller-Reichert, 2002; McDonald, 2007; Triffo et al., 2008). Specimens were flat-embedded between two microscopy slides and polymerized at 60℃ over 1 to 2 days. Resin-embedded samples were remounted under a dissecting microscope for precise orientation.

Transmission electron microscopy

70–100-nm sections were collected on formvar-coated grids using a Reichert Ultracut E ultramicrotome (Leica). Sections were post-stained using 2% uranyl acetate in 70% methanol followed by Sato's lead citrate. The sections were imaged in an FEI Tecnai 12 TEM (FEI, Eindhoven, The Netherlands) operated at 120 kV.

Montaged TEM Images

Owing to the large size of the samples, it was frequently necessary to collect multiple TEM images of overlapping adjacent areas to cover the relevant field of view at the necessary resolution. Montages of electron microscopy images were reconstructed using the freely available TrakEM2 program (Cardona et al., 2010; Saalfeld et al., 2010; Schmid et al., 2010). Images were aligned at full 2048 by 2048 pixel resolution and contrast was adjusted across adjacent images using TrakEm2. A custom Python script was written to assist in reconstruction. The montage function in TrakEM2 was applied, with further manual alignment as necessary. Overlaps were linear blended, and montages were exported as tiff files.

Serial block face and focused ion bean SEM sample preparation

Mouse mammary organoids were chemically fixed with 2.5% glutaraldehyde. To produce enough back-scatter electrons for SBF-SEM imaging, the organoids were stained with an osmium-thiocarbohydrazide-osmium (OTO) method (Friedman and Ellisman, 1981; Willingham and Rutherford, 1984), in combination with microwave-assisted processing. Organoids were rinsed three times with 0.1 M sodium cacodylate buffer and then incubated with solution of reduced 2% osmium

tetroxide (containing 1.5% potassium ferricyanide) in buffer. The samples were incubated using a Pelco Biowave microwave (Ted Pella Inc., Redding, CA) for 2 minutes at 150 watts of power. Following three rinses with buffer, the organoids were microwave for 40 seconds at 150 W in 0.1% thiocarbohydrazide in double-distilled water and then rinsed three times with water. Finally, they were microwaved for 1 minute at 150 watts with 2% osmium tetroxide and rinsed three times in water. To enhance preservation and contrast, the samples were high-pressure frozen as described for the TEM samples and freeze substituted with a solution of 4% osmium tetroxide, 0.1% uranyl acetate and 5% water in acetone. Following five rinses in pure acetone samples were infiltrated with hard-forming Epon resin with accelerator according to the following schedule: 2 hours in 2:1 acetone:resin; 2 hours in 1:1; 4 hours in 1:2; and overnight in pure resin. Samples were flat-embedded as described for the TEM samples. Representative SBF-SEM and FIB-SEM data series have been uploaded to the 'The Cell: An Image Library' (run by the ASCB; http://www.cellimagelibrary.org/).

Serial block face imaging

Organoids embedded in resin were mounted onto an aluminum pin with a cyanoacrylate adhesive. The pin, which takes the place of a normal SEM stub, was loaded into a sample holder for the Gatan 3View (Gatan, Pleasanton, CA). Serial block face scanning electron microscopy was carried out as previously described (Denk and Horstmann, 2004). Data were collected using an FEI Quanta 600 FEG SEM; serial images were 4k by 4k and acquired at 5 kV; *z*-dimension slices of 50 nm. 3D volume representations of the data were prepared using CHIMERA (Pettersen et al., 2004). CHIMERA was used to perform manual segmentation of membranes and to display the 3D volumes.

Focused ion beam SEM imaging

Resin-embedded samples were trimmed with a thin razor blade to expose the area of interest on both the top and one side of the block. This was then glued to a SEM stub using colloidal silver paint. Milling and imaging of the block was carried out using a FEI Strata 235 Dual Beam FIB (FEI, Hillsboro, OR). FIB milling at 50 pA generated a beam size of ~17 nm. 1k by 1k images were collected with a backscatter electron detector at 5 kV.

Antibody staining

Staining for E-cadherin (Zymed, 13-1900), ZO-1 (Chemicon, MAB1520), SMA (Sigma, F3777 or C6198), β-catenin (Santa Cruz Biotechnology, sc-7199), and aPKC-ζ (Santa Cruz Biotechnology, sc-216) was performed as previously reported (Ewald et al., 2008). Briefly, organoids were equilibrated in 25% sucrose in PBS for 1 hour, fixed in cold 1:1 methanol:acetone overnight at –20℃, then re-equilibrated in 25% sucrose in PBS for 1 hour. Samples were blocked 1 hour with 5% serum, incubated with primary antibody (all 1:250 in PBS) for two hours to overnight and rinsed three times in PBS. For PAR3 (Millipore, catalog number 07-330), numb (Cell Signaling Technology, C29611) and scribble (Santa Cruz Biotechnology, sc-11049) staining, organoids were fixed in 4% PFA for 20 minutes and permeabilized in 0.5% Triton X-100 for 30 minutes. Samples were blocked in 10% serum for 3 hours, incubated with primary antibody (all 1:500 in 10% serum) for two hours to overnight and rinsed three times in 10% serum. Secondary Alexa-Fluor-conjugated antibodies (Molecular Probes, all 1:250 in PBS) were incubated with the organoids for 1–4 hours. Nuclei were stained with DAPI or propidium iodide (1:1000) (Molecular Probes). Antibody stains were performed at least three independent times, inspecting a minimum of 25 organoids in each condition each time.

Confocal imaging

Confocal imaging was performed on a Solamere Technology Group spinning disk confocal microscope as described previously (Ewald, 2010), with a 40× C-Apochromat objective lens (Zeiss Microimaging). Acquisition of both fixed and time-lapse images was performed using a combination of μManager (Edelstein et al., 2010) and Piper (Stanford Photonics). Levels were adjusted in Adobe Photoshop to maximize clarity of the images. Level adjustments were always done on the entire image.

Single-cell labeling with adenoviral GFP

Epithelial fragments were prepared using the previously described organotypic culture method. Before resuspension in Matrigel 1000 organoids in 500 μl DMEM F12 were transferred to a 1.7 ml Eppendorf tube. The tube was then pulsed at 520 ***g*** for 30 seconds. Medium was removed from the pellet and organoids were resuspended in 50 μl DMEM F12. Ad-CMV-GFP (Vector Biolabs, 1060) was then added at a ratio of 2000 or 10,000 plaque-forming units (pfu):organoid. Epithelial fragments were incubated with virus for 1.5 hours at 37℃ and washed three times in DMEM F12. Organoids were then resuspended in Matrigel and plated as described above.

Time-lapse microscopy

Time-lapse movies were recorded for 5–7 days during which time the temperature was held at 37℃ and humidity was held at 5%. Images were acquired every 10 minutes for a duration of 8–24 hours and 10–30 movies were collected in parallel. Imaris (Bitplane) was used for image analysis. CellTracker was used to label organoids as described previously (Ewald et al., 2008).

Image processing

Surface rendering and single-cell tracking were generated using the Imaris (Bitplane) IsoSurfaces function. Before surface rendering a gaussian smoothing filter with width of 1 voxel was applied and background signal was subtracted. A minimum intensity filter and a minimum voxel size filter were manually adjusted such that the rendered surface visually matched the surface area of individual cells. IsoSurfaces were tracked using the autoregressive motion algorithm with a maximum distance of 5 μm and a maximum gap of three frames. The mean cell speed was calculated as the total track length divided by the time.

Acknowledgements

We thank Dr. Kent McDonald (UC Berkeley EM Lab) for his advice and assistance in sample preparation. We thank Chris Booth (Gatan, Inc.), Joel Mancuso (Gatan, Inc.), and Tom Goddard (UCSF), for their advice in sample preparation, 3View data collection, and 3D visualization respectively. We thank Chris Mitchell (JHMI) for assistance in image processing. We thank Carl Zeiss Microimaging, The Molecular Foundry at the Lawrence Berkeley Lab, and the National Center for Electron Microscopy for assistance in pilot 3D FIB-SEM studies. AJE thanks Paul Matsudaira for suggesting the possibility that the lateral membrane protrusions represented 3D membrane extensions.

Funding

This work was supported by funds from the National Cancer Institute [grant number P50 CA88843]; the National Heart, Lung, and Blood Institute [grant number R01 HL107361]; and the Safeway Foundation Award for Breast Cancer Research to A.J.E.; by the Director, Office of Science, of the U.S. Department of Energy [contract DE-AC03-76SF00098] to M.A.; by the University of California – Berkeley Physical Sciences in Oncology Center to M.A. and D.M.J.; and the National Cancer Institute and National Institute of Environmental Health Sciences [grant numbers R01 CA057621, U01 ES019458] and the California Breast Cancer Research Program [grant number 17UB-8705] to Z.W.

Supplementary material available online at
http://jcs.biologists.org/lookup/suppl/doi:10.1242/jcs.096875/-/DC1

References

Berx, G., Cleton-Jansen, A. M., Strumane, K., de Leeuw, W. J., Nollet, F., van Roy, F. and Cornelisse, C. (1996). E-cadherin is inactivated in a majority of invasive human lobular breast cancers by truncation mutations throughout its extracellular domain. *Oncogene* **13**, 1919-1925.

Bilder, D., Li, M. and Perrimon, N. (2000). Cooperative regulation of cell polarity and growth by Drosophila tumor suppressors. *Science* **289**, 113-116.

Bogenrieder, T. and Herlyn, M. (2003). Axis of evil: molecular mechanisms of cancer metastasis. *Oncogene* **22**, 6524-6536.

Cardona, A., Saalfeld, S., Preibisch, S., Schmid, B., Cheng, A., Pulokas, J., Tomancak, P. and Hartenstein, V. (2010). An integrated micro- and macro-architectural analysis of the Drosophila brain by computer-assisted serial section electron microscopy. *PLoS Biol.* **8**, e1000502.

Chepko, G. and Smith, G. H. (1997). Three division-competent, structurally-distinct cell populations contribute to murine mammary epithelial renewal. *Tissue Cell* **29**, 239-253.

Chepko, G. and Smith, G. H. (1999). Mammary epithelial stem cells: our current understanding. *J. Mammary Gland Biol. Neoplasia* **4**, 35-52.

Chi, X., Michos, O., Shakya, R., Riccio, P., Enomoto, H., Licht, J. D., Asai, N., Takahashi, M., Ohgami, N., Kato, M. et al. (2009). Ret-dependent cell rearrangements in the Wolffian duct epithelium initiate ureteric bud morphogenesis. *Dev. Cell* **17**, 199-209.

Conacci-Sorrell, M., Zhurinsky, J. and Ben-Ze'ev, A. (2002). The cadherin-catenin adhesion system in signaling and cancer. *J. Clin. Invest.* **109**, 987-991.

Cui, T., Chen, Y., Yang, L., Knösel, T., Zöller, K., Huber, O. and Petersen, I. (2011). DSC3 expression is regulated by p53, and methylation of DSC3 DNA is a prognostic marker in human colorectal cancer. *Br. J. Cancer* **104**, 1013-1019.

Daniel, C. W., De Ome, K. B., Young, J. T., Blair, P. B. and Faulkin, L. J., Jr (1968). The in vivo life span of normal and preneoplastic mouse mammary glands: a serial transplantation study. *Proc. Natl. Acad. Sci. USA* **61**, 53-60.

Den, Z. N., Cheng, X., Merched-Sauvage, M. and Koch, P. J. (2006). Desmocollin 3 is required for pre-implantation development of the mouse embryo. *J. Cell Sci.* **119**, 482-489.

Denk, W. and Horstmann, H. (2004). Serial block-face scanning electron microscopy to reconstruct three-dimensional tissue nanostructure. *PLoS Biol.* **2**, e329.

Derksen, P. W., Liu, X., Saridin, F., van der Gulden, H., Zevenhoven, J., Evers, B., van Beijnum, J. R., Griffioen, A. W., Vink, J., Krimpenfort, P. et al. (2006). Somatic inactivation of E-cadherin and p53 in mice leads to metastatic lobular mammary carcinoma through induction of anoikis resistance and angiogenesis. *Cancer Cell* **10**, 437-449.

Derksen, P. W., Braumuller, T. M., van der Burg, E., Hornsveld, M., Mesman, E., Wesseling, J., Krimpenfort, P. and Jonkers, J. (2011). Mammary-specific inactivation of E-cadherin and p53 impairs functional gland development and leads to pleomorphic invasive lobular carcinoma in mice. *Dis. Model. Mech.* **4**, 347-358.

Dusek, R. L. and Attardi, L. D. (2011). Desmosomes: new perpetrators in tumour suppression. *Nat. Rev. Cancer* **11**, 317-323.

Edelstein, A., Amodaj, N., Hoover, K., Vale, R. and Stuurman, N. (2010). Computer control of microscopes using microManager. *Curr. Protoc. Mol. Biol.* **14**, 20.

Ewald, A. J. (2010). Practical considerations for long-term time-lapse imaging of epithelial morphogenesis in three-dimensional organotypic cultures. In *Imaging in Developmental Biology* (ed. R. Wong and J. Sharpe). New York: Cold Spring Harbor Laboratory Press.

Ewald, A. J., Brenot, A., Duong, M., Chan, B. S. and Werb, Z. (2008). Collective epithelial migration and cell rearrangements drive mammary branching morphogenesis. *Dev. Cell* **14**, 570-581.

Fata, J. E., Mori, H., Ewald, A. J., Zhang, H., Yao, E., Werb, Z. and Bissell, M. J. (2007). The MAPK(ERK-1,2) pathway integrates distinct and antagonistic signals from TGFalpha and FGF7 in morphogenesis of mouse mammary epithelium. *Dev. Biol.* **306**, 193-207.

Feigin, M. E. and Muthuswamy, S. K. (2009). Polarity proteins regulate mammalian cell-cell junctions and cancer pathogenesis. *Curr. Opin. Cell Biol.* **21**, 694-700.

Friedman, P. L. and Ellisman, M. H. (1981). Enhanced visualization of peripheral nerve and sensory receptors in the scanning electron microscope using cryofracture and osmium-thiocarbohydrazide-osmium impregnation. *J. Neurocytol.* **10**, 111-131.

Getsios, S., Huen, A. C. and Green, K. J. (2004). Working out the strength and flexibility of desmosomes. *Nat. Rev. Mol. Cell Biol.* **5**, 271-281.

Goldenberg, V. E., Goldenberg, N. S. and Sommers, S. C. (1969). Comparative ultrastructure of atypical ductal hyperplasia, intraductal carcinoma, and infiltrating ductal carcinoma of the breast. *Cancer* **24**, 1152-1169.

Gönczy, P. (2008). Mechanisms of asymmetric cell division: flies and worms pave the way. *Nat. Rev. Mol. Cell Biol.* **9**, 355-366.

Green, K. J. and Gaudry, C. A. (2000). Are desmosomes more than tethers for intermediate filaments? *Nat. Rev. Mol. Cell Biol.* **1**, 208-216.

Gumbiner, B., Stevenson, B. and Grimaldi, A. (1988). The role of the cell adhesion molecule uvomorulin in the formation and maintenance of the epithelial junctional complex. *J. Cell Biol.* **107**, 1575-1587.

Hanson, P., Mathews, V., Marrus, S. H. and Graubert, T. A. (2003). Enhanced green fluorescent protein targeted to the Sca-1 (Ly-6A) locus in transgenic mice results in efficient marking of hematopoietic stem cells in vivo. *Exp. Hematol.* **31**, 159-167.

Hendrix, M. J., Seftor, E. A., Seftor, R. E., Kasemeier-Kulesa, J., Kulesa, P. M. and Postovit, L. M. (2007). Reprogramming metastatic tumour cells with embryonic microenvironments. *Nat. Rev. Cancer* **7**, 246-255.

Hennighausen, L. and Robinson, G. W. (2005). Information networks in the mammary gland. *Nat. Rev. Mol. Cell Biol.* **6**, 715-725.

Hinck, L. and Silberstein, G. B. (2005). Key stages in mammary gland development: the mammary end bud as a motile organ. *Breast Cancer Res.* **7**, 245-251.

Hirohashi, S. (1998). Inactivation of the E-cadherin-mediated cell adhesion system in human cancers. *Am. J. Pathol.* **153**, 333-339.

Hogg, N. A., Harrison, C. J. and Tickle, C. (1983). Lumen formation in the developing mouse mammary gland. *J. Embryol. Exp. Morphol.* **73**, 39-57.

Huang, L. and Muthuswamy, S. K. (2010). Polarity protein alterations in carcinoma: a focus on emerging roles for polarity regulators. *Curr. Opin. Genet. Dev.* **20**, 41-50.

Ihrie, R. A. and Attardi, L. D. (2005). A new Perp in the lineup: linking p63 and desmosomal adhesion. *Cell Cycle* **4**, 873-876.

Ingber, D. E. (2008). Can cancer be reversed by engineering the tumor microenvironment? *Semin. Cancer Biol.* **18**, 356-364.

Jeanes, A., Gottardi, C. J. and Yap, A. S. (2008). Cadherins and cancer: how does cadherin dysfunction promote tumor progression? *Oncogene* **27**, 6920-6929.

Kalluri, R. and Weinberg, R. A. (2009). The basics of epithelial-mesenchymal transition. *J. Clin. Invest.* **119**, 1420-1428.

Keller, R. (2002). Shaping the vertebrate body plan by polarized embryonic cell movements. *Science* **298**, 1950-1954.

Klus, G. T., Rokaeus, N., Bittner, M. L., Chen, Y. D., Korz, D. M., Sukumar, S., Schick, A. and Szallasi, Z. (2001). Down-regulation of the desmosomal cadherin desmocollin 3 in human breast cancer. *Int. J. Oncol.* **19**, 169-174.

Knudsen, K. A. and Wheelock, M. J. (2005). Cadherins and the mammary gland. *J. Cell. Biochem.* **95**, 488-496.

Langbein, L., Grund, C., Kuhn, C., Praetzel, S., Kartenbeck, J., Brandner, J. M., Moll, I. and Franke, W. W. (2002). Tight junctions and compositionally related junctional structures in mammalian stratified epithelia and cell cultures derived therefrom. *Eur. J. Cell Biol.* **81**, 419-435.

Larsen, M., Wei, C. and Yamada, K. M. (2006). Cell and fibronectin dynamics during branching morphogenesis. *J. Cell Sci.* **119**, 3376-3384.

Larue, L., Ohsugi, M., Hirchenhain, J. and Kemler, R. (1994). E-cadherin null mutant embryos fail to form a trophectoderm epithelium. *Proc. Natl. Acad. Sci. USA* **91**, 8263-8267.

Lauffenburger, D. A. and Horwitz, A. F. (1996). Cell migration: a physically integrated molecular process. *Cell* **84**, 359-369.

Lechler, T. and Fuchs, E. (2007). Desmoplakin: an unexpected regulator of microtubule organization in the epidermis. *J. Cell Biol.* **176**, 147-154.

Lee, K., Gjorevski, N., Boghaert, E., Radisky, D. C. and Nelson, C. M. (2011). Snail1, Snail2, and E47 promote mammary epithelial branching morphogenesis. *EMBO J.* **30**, 2662-2674.

Lu, P., Ewald, A. J., Martin, G. R. and Werb, Z. (2008). Genetic mosaic analysis reveals FGF receptor 2 function in terminal end buds during mammary gland branching morphogenesis. *Dev. Biol.* **321**, 77-87.

Mailleux, A. A., Overholtzer, M., Schmelzle, T., Bouillet, P., Strasser, A. and Brugge, J. S. (2007). BIM regulates apoptosis during mammary ductal morphogenesis, and its absence reveals alternative cell death mechanisms. *Dev. Cell* **12**, 221-234.

McDonald, K. (2007). Cryopreparation methods for electron microscopy of selected model systems. *Methods Cell Biol.* **79**, 23-56.

McDonald, K. and Müller-Reichert, T. (2002). Cryomethods for thin section electron microscopy. *Methods Enzymol.* **351**, 96-123.

McDonald, K. L. and Auer, M. (2006). High-pressure freezing, cellular tomography, and structural cell biology. *Biotechniques* **41**, 137-143.

Nanba, D., Nakanishi, Y. and Hieda, Y. (2001). Changes in adhesive properties of epithelial cells during early morphogenesis of the mammary gland. *Dev. Growth Differ.* **43**, 535-544.

Nelson, C. M. and Bissell, M. J. (2006). Of extracellular matrix, scaffolds, and signaling: tissue architecture regulates development, homeostasis, and cancer. *Annu. Rev. Cell Dev. Biol.* **22**, 287-309.

Nelson, W. J. (2009). Remodeling epithelial cell organization: transitions between front-rear and apical-basal polarity. *Cold Spring Harb. Perspect. Biol.* **1**, a000513.

O'Brien, L. E., Zegers, M. M. and Mostov, K. E. (2002). Opinion: Building epithelial architecture: insights from three-dimensional culture models. *Nat. Rev. Mol. Cell Biol.* **3**, 531-537.

Oshiro, M. M., Kim, C. J., Wozniak, R. J., Junk, D. J., Muñoz-Rodríguez, J. L., Burr, J. A., Fitzgerald, M., Pawar, S. C., Cress, A. E., Domann, F. E. et al. (2005). Epigenetic silencing of DSC3 is a common event in human breast cancer. *Breast Cancer Res.* **7**, R669-R680.

Ozzello, L. (1971). Ultrastructure of the human mammary gland. *Pathol. Annu.* **6**, 1-59.

Pagliarini, R. A. and Xu, T. (2003). A genetic screen in Drosophila for metastatic behavior. *Science* **302**, 1227-1231.

Pagliarini, R. A., Quiñones, A. T. and Xu, T. (2003). Analyzing the function of tumor suppressor genes using a Drosophila model. *Methods Mol. Biol.* **223**, 349-382.

Petersen, O. W., Rønnov-Jessen, L., Howlett, A. R. and Bissell, M. J. (1992). Interaction with basement membrane serves to rapidly distinguish growth and differentiation pattern of normal and malignant human breast epithelial cells. *Proc. Natl. Acad. Sci. USA* **89**, 9064-9068.

Pettersen, E. F., Goddard, T. D., Huang, C. C., Couch, G. S., Greenblatt, D. M., Meng, E. C. and Ferrin, T. E. (2004). UCSF Chimera–a visualization system for exploratory research and analysis. *J. Comput. Chem.* **25**, 1605-1612.

Pitelka, D. R., Hamamoto, S. T., Duafala, J. G. and Nemanic, M. K. (1973). Cell contacts in the mouse mammary gland. I. Normal gland in postnatal development and the secretory cycle. *J. Cell Biol.* **56**, 797-818.

Polyak, K. and Weinberg, R. A. (2009). Transitions between epithelial and mesenchymal states: acquisition of malignant and stem cell traits. *Nat. Rev. Cancer* **9**, 265-273.

Rosen, P. P. (2001). *Rosen's Breast Pathology*. Philadelphia, PA: Lippincott Williams and Wilkins.

Rudland, P. S. (1991). Histochemical organization and cellular composition of ductal buds in developing human breast: evidence of cytochemical intermediates between epithelial and myoepithelial cells. *J. Histochem. Cytochem.* **39**, 1471-1484.

Runswick, S. K., O'Hare, M. J., Jones, L., Streuli, C. H. and Garrod, D. R. (2001). Desmosomal adhesion regulates epithelial morphogenesis and cell positioning. *Nat. Cell Biol.* **3**, 823-830.

Saalfeld, S., Cardona, A., Hartenstein, V. and Tomancák, P. (2010). As-rigid-as-possible mosaicking and serial section registration of large ssTEM datasets. *Bioinformatics* **26**, i57-i63.

Schmid, B., Schindelin, J., Cardona, A., Longair, M. and Heisenberg, M. (2010). A high-level 3D visualization API for Java and ImageJ. *BMC Bioinformatics* **11**, 274.

Schneeberger, E. E. and Lynch, R. D. (2004). The tight junction: a multifunctional complex. *Am. J. Physiol. Cell Physiol.* **286**, C1213-C1228.

Simian, M., Hirai, Y., Navre, M., Werb, Z., Lochter, A. and Bissell, M. J. (2001). The interplay of matrix metalloproteinases, morphogens and growth factors is necessary for branching of mammary epithelial cells. *Development* **128**, 3117-3131.

Smith, G. H. and Medina, D. (1988). A morphologically distinct candidate for an epithelial stem cell in mouse mammary gland. *J. Cell Sci.* **90**, 173-183.

Smith, G. H. and Chepko, G. (2001). Mammary epithelial stem cells. *Microsc. Res. Tech.* **52**, 190-203.

Sosinsky, G. E., Crum, J., Jones, Y. Z., Lanman, J., Smarr, B., Terada, M., Martone, M. E., Deerinck, T. J., Johnson, J. E. and Ellisman, M. H. (2008). The

Journal of Cell Science

combination of chemical fixation procedures with high pressure freezing and freeze substitution preserves highly labile tissue ultrastructure for electron tomography applications. *J. Struct. Biol.* **161**, 359-371.

Sternlicht, M. D. (2006). Key stages in mammary gland development: the cues that regulate ductal branching morphogenesis. *Breast Cancer Res.* **8**, 201.

Sternlicht, M. D., Sunnarborg, S. W., Kouros-Mehr, H., Yu, Y., Lee, D. C. and Werb, Z. (2005). Mammary ductal morphogenesis requires paracrine activation of stromal EGFR via ADAM17-dependent shedding of epithelial amphiregulin. *Development* **132**, 3923-3933.

Stirling, J. W. and Chandler, J. A. (1976). The fine structure of the normal, resting terminal ductal-lobular unit of the female breast. *Virchows Arch. A Pathol. Anat. Histol.* **372**, 205-226.

Stirling, J. W. and Chandler, J. A. (1977). The fine structure of ducts and subareolar ducts in the resting gland of the female breast. *Virchows Arch. A Pathol. Anat. Histol.* **373**, 119-132.

Streuli, C. H., Bailey, N. and Bissell, M. J. (1991). Control of mammary epithelial differentiation: basement membrane induces tissue-specific gene expression in the absence of cell-cell interaction and morphological polarity. *J. Cell Biol.* **115**, 1383-1395.

Stubbs, J. L., Davidson, L., Keller, R. and Kintner, C. (2006). Radial intercalation of ciliated cells during Xenopus skin development. *Development* **133**, 2507-2515.

Triffo, W. J., Palsdottir, H., McDonald, K. L., Lee, J. K., Inman, J. L., Bissell, M. J., Raphael, R. M. and Auer, M. (2008). Controlled microaspiration for high-pressure freezing: a new method for ultrastructural preservation of fragile and sparse tissues for TEM and electron tomography. *J. Microsc.* **230**, 278-287.

Underwood, J. M., Imbalzano, K. M., Weaver, V. M., Fischer, A. H., Imbalzano, A. N. and Nickerson, J. A. (2006). The ultrastructure of MCF-10A acini. *J. Cell. Physiol.* **208**, 141-148.

Vasioukhin, V., Bowers, E., Bauer, C., Degenstein, L. and Fuchs, E. (2001). Desmoplakin is essential in epidermal sheet formation. *Nat. Cell Biol.* **3**, 1076-1085.

Wang, Z., Sandiford, S., Wu, C. and Li, S. S. (2009). Numb regulates cell-cell adhesion and polarity in response to tyrosine kinase signalling. *EMBO J.* **28**, 2360-2373.

Weaver, V. M., Petersen, O. W., Wang, F., Larabell, C. A., Briand, P., Damsky, C. and Bissell, M. J. (1997). Reversion of the malignant phenotype of human breast cells in three-dimensional culture and in vivo by integrin blocking antibodies. *J. Cell Biol.* **137**, 231-245.

Weigelt, B. and Bissell, M. J. (2008). Unraveling the microenvironmental influences on the normal mammary gland and breast cancer. *Semin. Cancer Biol.* **18**, 311-321.

Williams, J. M. and Daniel, C. W. (1983). Mammary ductal elongation: differentiation of myoepithelium and basal lamina during branching morphogenesis. *Dev. Biol.* **97**, 274-290.

Willingham, M. C. and Rutherford, A. V. (1984). The use of osmium-thiocarbohydrazide-osmium (OTO) and ferrocyanide-reduced osmium methods to enhance membrane contrast and preservation in cultured cells. *J. Histochem. Cytochem.* **32**, 455-460.

Wiseman, B. S., Sternlicht, M. D., Lund, L. R., Alexander, C. M., Mott, J., Bissell, M. J., Soloway, P., Itohara, S. and Werb, Z. (2003). Site-specific inductive and inhibitory activities of MMP-2 and MMP-3 orchestrate mammary gland branching morphogenesis. *J. Cell Biol.* **162**, 1123-1133.

Yang, J. and Weinberg, R. A. (2008). Epithelial-mesenchymal transition: at the crossroads of development and tumor metastasis. *Dev. Cell* **14**, 818-829.